



CHALMERS
UNIVERSITY OF TECHNOLOGY

Model Based Development of Mild Hybrid Electrical Battery Systems

Master of Science Thesis

**MOHANAPRIYA ANANDAGURU
ANDREAS ERIKSSON**

MASTER OF SCIENCE THESIS REPORT

**Model Based Development of Hybrid Electrical Battery
Systems**

MOHANAPRIYA ANANDAGURU
ANDREAS ERIKSSON



CHALMERS
UNIVERSITY OF TECHNOLOGY

Department of Electric Power Engineering
Division of Electric Power Engineering
CHALMERS UNIVERSITY OF TECHNOLOGY
Gothenburg, Sweden 2018

Model Based Development of Hybrid Electrical Battery Systems
© MOHANAPRIYA ANANDAGURU
ANDREAS ERIKSSON, 2018.

Supervisors:

Linus Brusokas, Volvo Car Corporation
Torbjörn Larsson, Volvo Car Corporation
Stefan Skoog, Electric Power Engineering

Examiner: Torbjörn Thiringer, Electric Power Engineering

Master's Thesis Report
Department of Electric Power Engineering
Division of Electric Power Engineering
Chalmers University of Technology
SE-412 96 Gothenburg
Telephone +46 31 772 1000

Typeset in L^AT_EX
Printed by [Chalmers Reproservice]
Gothenburg, Sweden 2018

Abstract

In this thesis, a battery energy storage model is developed for a 48 V Mild Hybrid system in the MATLAB/Simulink environment. The battery energy storage model consists of an electrical model, a thermal model and a SOC estimator. The electrical model is based on equivalent circuit models where both 0RC, 1RC and 2RC model parameters are extracted from measurements on individual cells. The thermal model is based on a 1D lumped parameter model including the thermal resistance from the battery pack to the environment and the thermal mass of the battery pack. The SOC estimator is based on current integration. The battery model is evaluated during different driving cycles and the electrical models are compared in terms of accuracy. Finally the battery energy storage model is implemented in a simplified 48 V mild hybrid system together with an ISGM model and is evaluated in terms of electrical and thermal behaviour.

The electro-thermal battery model shows good accuracy for a double WLTP driving cycle, with a voltage RMSE value around 1% and a maximum error of 6% which occurred at low temperatures. When comparing the 2RC and 1RC electrical models, it shows that they have similar performance. The thermal model shows an RMSE of 1-2 °C and a maximum temperature error of 5 °C for the WLTP driving cycles. The SOC estimator shows a RMSE of 1% and a maximum error of 2%.

Keywords: Mild Hybrid, Electro-Thermal, 48V, battery modelling, Li-ion battery, Equivalent circuit models.

Acknowledgements

Firstly, we would like to extend our special thanks of gratitude to our supervisor Stefan Skoog for his valuable feedback, suggestions and encouragement in completing our project successfully. We would also like to express our thanks to our examiner Professor Torbjörn Thiringer for his support and help. Further we also like to thank our supervisors Linas Brusokas and Torbjörn Larsson at Volvo Car Corporation for their time and commitment in guiding us for the success of the project. A special thanks to our manager Alexander Robertsson for giving us an opportunity to do our thesis at Volvo Cars.

Mohanapriya and Andreas, Gothenburg, June 2018

Contents

1	Introduction	1
1.1	Problem background	1
1.2	Previous work	2
1.3	Purpose	3
2	Theory	5
2.1	Mild hybrid electric vehicles architecture	5
2.2	Battery Terminologies	7
2.3	Battery modeling	8
2.4	Voltage response to discharge pulse	9
2.5	Equivalent-Circuit Models	9
2.5.1	Ideal voltage source	10
2.5.2	0RC model	10
2.5.3	1RC model	10
2.5.4	2RC model	11
2.6	Electrical model parameter extraction	12
2.7	State of Charge estimation	13
2.8	48 V Battery pack	14
2.9	Temperature Modeling	15
2.9.1	1D lumped-parameter method	16
2.10	Root-Mean-Square Error (RMSE)	16
2.11	WLTP	17
3	Method	19
3.1	Extracting electrical model parameters	19
3.1.1	Laboratory tests	20
3.1.2	Curve Fitting	22
3.2	Component model implementation in Simulink	24
3.2.1	Electrical cell model	24
3.2.2	Electrical Battery Pack Model	26
3.2.3	Electro-thermal Cell Model	28
3.3	48 V system simulation	29
4	Results	31
4.1	Cell Capacity	31
4.2	Equivalent circuit model parameters	32

4.2.1	Equivalent resistance	32
4.2.2	2RC Model parameters	33
4.2.3	1RC Model parameters	36
4.3	Model Verification	36
4.4	Battery Pack Simulations	40
4.5	System Simulations	42
5	Conclusion	45
5.1	Cell chemistry comparison	45
5.2	Electro-thermal battery pack model evaluation	45
5.3	Sustainable aspects	45
5.4	Ethics	46
5.5	Future work	46
	Bibliography	47

Abbreviations

CO_2	Carbon dioxide
NO_x	Nitrogen oxide
ABS	Antilocking Braking System
BEV	Battery Electric Vehicle
BiSG	Belt driven integrated Stator Generator
ECM	Equivalent Circuit Model
ESR	Equivalent Series Resistance
FEAD	Front End Accessory Drive
HEV	Hybrid Electric Vehicle
ICCT	International Council on clean Transportation
ICE	Internal Combustion Engine
LTO	Lithium-titanate
MHEV	Mild Hybrid Electric Vehicle
NMC	Lithium Nickel Manganese Cobalt Oxide
OCV	Open Circuit Voltage
PHEV	Plug in Hybrid vehicle
RMSE	Root Mean Square Error
SOA	Safe Operating Area
SOC	State of Charge
VCC	Volvo Car Corporation
WLTP	Worldwide Harmonised Light Vehicle Test Procedure

1

Introduction

1.1 Problem background

At present, the concern to reduce greenhouse gases are increasing rapidly world wide. One of the major sources of these polluting gases, such as CO_2 and NOx , are due to the emissions from the vehicle fleet. As a result, International Council on Clean Transportation (ICCT) enacted laws and regulations to reduce the average vehicle fleet emissions to 95 grams of CO_2 per kilometer by 2021 [1]. This has raised the pressure on the vehicle manufacturers to find new technological solutions to meet these requirements. Hence many manufacturers have started Hybrid Electric Vehicle (HEV) programs as one of the solutions to meet these emission goals. Figure 1.1 shows the details on electrification strategies used by car manufacturers on a scale from the pure Internal Combustion Engine (ICE) vehicle to the fully electrified vehicle [2].

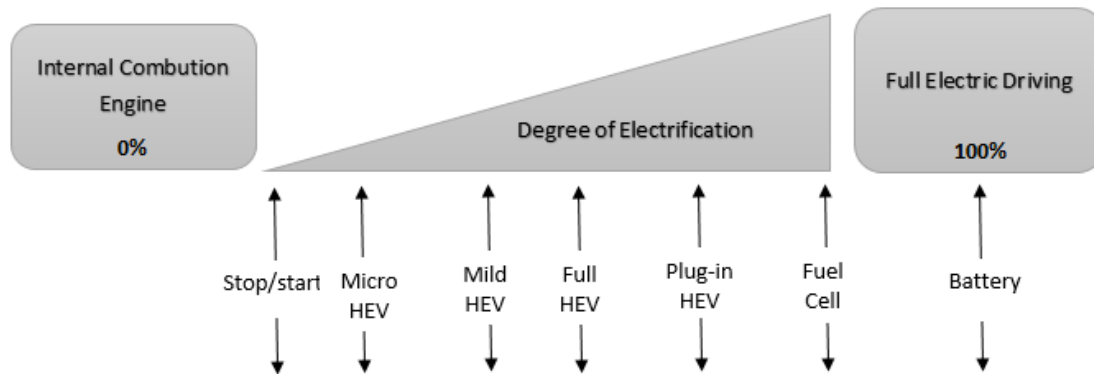


Figure 1.1: Degree of Electrification

Plug-in hybrid (PHEV) and HEV are the vehicles that use at least two power sources and have an electrical machine integrated with the conventional ICE to provide torque assistance. The main difference between a PHEV and a HEV is that a PHEV can be recharged by an external electric power source. Some features of a hybrid car that improves fuel economy are regenerative braking, start-stop system and propulsion assistance. Instead of friction braking which dissipates energy during slight deceleration, regenerative braking can be utilized. Regenerative braking allows the car to recover energy during deceleration by using the electrical machine as

a generator. Automatic start-stop system turns off the ICE during stand still when no propulsion power is required and therefore reduces wasted energy from idling. The electrical machine can also provide assistance to the ICE when accelerating or while driving at low speed where ICEs are least efficient [3].

Volvo Car Corporation (VCC) currently offers plug-in hybrids with their Twin Engine motor concept as well as cars with conventional ICEs. In order to respond to the increasing demand on electrified cars, VCC has developed a mild hybrid electric propulsion system which is a cost-reduced 48 V-based electrification strategy. The mild hybrid should bridge the gap between plug-in hybrids and ICE cars. The 48 V-based electrification strategy has the potential to suit most car models and offers many important benefits from full hybrids such as regenerative braking, automatic start-stop system and torque assist, but at a lower cost [4]. VCC aims to electrify the entire car fleet by 2019, and the mild hybrids with 48 V systems will be the lowest priced product family [5].

As the 48 V mild hybrid system is a new technology, there is still a need for further research and development before it can reach its full potential. There is a large need to study both the electrical and drive cycle behavior down to the component level in the 48 V board net. One of the key components in the mild hybrid system concept is the 48 V battery pack which supplies both the 48 V loads and electrical machine as well as store energy during recuperation. The battery pack also takes care of transient events and provides voltage stability. As a consequence, the battery pack quality needs to be continuously tested and improved in order to meet customers requirements. Testing the electrical systems of the cars with physical batteries is not always an option early in the development process and it is also time consuming, expensive and resource intensive. Therefore, the availability of accurate battery pack models for simulation is crucial for the development and quality insurance of the electrical system.

1.2 Previous work

Previous work has been done at the Division of Electric Power Engineering at Chalmers University of Technology together with VCC. Akik Biswas and Xuming Yao, master thesis students of 2016, developed an electro-thermal battery pack model using GTSUITE®. They investigated the effect of joule and entropic heat on the total heat dissipation from the battery pack and their influence on the battery pack temperature. They also compared the model accuracy of a 2RC circuit and a 0RC circuit model. In their thesis the 2RC circuit model produced an error of 1.5%, while the 0RC circuit model gave an error of 3.2%. Simulation time for the 0RC model was approximately 4 minutes, while for 2RC model, the simulation time exceeded 20 minutes [6].

Another work relate to parameterization of equivalent circuit model for Li-ion batteries, was carried out by Stefan Skoog. The aim of this work was to estimate the battery terminal voltage and RMSE value using open loop electrical model. The

model comparison was carried out with the real load cycle from the hybrid electric vehicle. In this work the 2RC model produced an RMSE of 10.65 mV while the 1RC model gave a voltage error of 26.25mV and the 0RC model shows 28.4 mV error value [18].

1.3 Purpose

The purpose of this thesis work is to develop accurate and efficient electro-thermal battery pack models of a 48 V Li-ion battery pack. The models should be compatible with VCC's simulation environment, provide RMSE voltage error less than 1.5% of the nominal voltage and render accurate temperature estimations with fast simulation time compared to [6]. Further, the aim is to evaluate the model in a simplified 48 V mild hybrid system during transient and steady-state scenarios.

2

Theory

2.1 Mild hybrid electric vehicles architecture

The increasing requirements in vehicle power supply have taken the traditional 12 V power supply to its limits. Therefore, to be able to meet the higher power supply demands, car manufacturers has started to introduce a second voltage level at 48 V [9]. The 48 V hybrid system is one of the solutions as it provides higher electric power than the 12 V system with lower current, thus requiring smaller diameter of current carrying conductor and lighter harnesses, which in turn reduces the losses and increases efficiency [10].

The main 48 V components of a mild hybrid vehicle are the electrical machine, the inverter (usually integrated with the electrical machine), the DC/DC converter and the 48 V battery pack. The mild hybrid features a dual 48 V/12V net topology which is shown in figure 2.1 [13]. The 48 V systems can supply the high power loads such as electric machines, power steering and the electric water pump. The 12 V system supplies the minor loads such as the chassis control system, infotainment, door locks, radios and lights [9]. The 48 V system is connected to the 12 V system by a DC/DC converter which allows for the 48 V board net to supply electric power to the 12 V system.

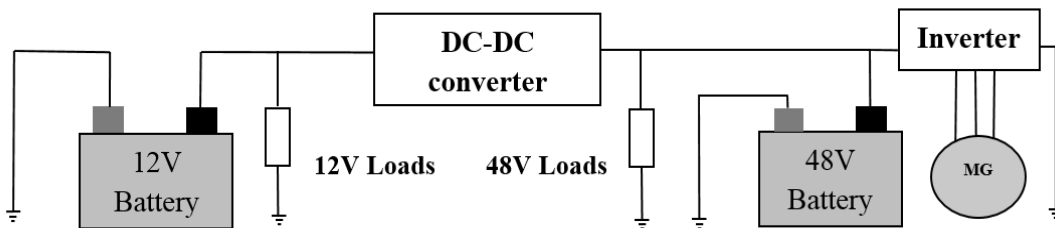


Figure 2.1: Schematic diagram of a 48 V system

Figure 2.2 shows different electrical machine positions for the 48 V Mild Hybrid system [11].

- P0: The machine is connected to ICE on the Front End Accessory Drive (FEAD).
- P1: The machine is connected with ICE directly with the crankshaft

2. Theory

- P2: The machine is integrated between the ICE and transmission shaft.
- P3: The machine is placed in the transmission shaft through gear mesh.
- P4: The machine is connected to the rear axle of the vehicle through gear mesh.

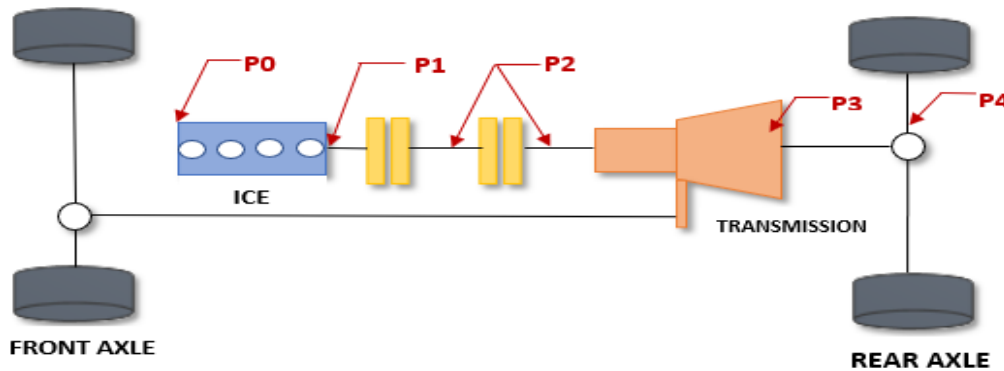


Figure 2.2: MHEV architecture

The different configurations provide different features of the Mild Hybrid. Some features of the P0 and P1 configuration include start-stop system, torque assistance and brake regeneration. The main difference between P2 and P0/P1 configuration is that P2 has higher increased energy recuperation potential and more effective torque boosting. This is because P0/P1 have the electric machines on the engine side and therefore it is not possible to mechanically disconnect it from the ICE, as a consequence torque losses occur.

Compared to P2, the P3/P4 configurations have the potential for electric driving mode. The P4 configuration could even provide all wheel drive mode. The increase in fuel efficiency during one WLTP cycle for the P0/P1 is 7%-9% while for P2, P3 and P4 it is 14%-16% according to [8]. The cheapest topology is P0 due to the limited impact of the 48 V system on the ICE [8].

Figure 2.3 shows the voltage limits according to excerpt from VDA 320 standards which is used by vehicle manufacturers. The 48 V operating condition is considered as the acceptable level for operating vehicles as it provides an additional guard band thus avoiding 60 V shock threshold and hence do not require extra protection for human operators or vehicle manufacturers [14]. Consequently, additional protection equipment increases the cost of the vehicle [15].

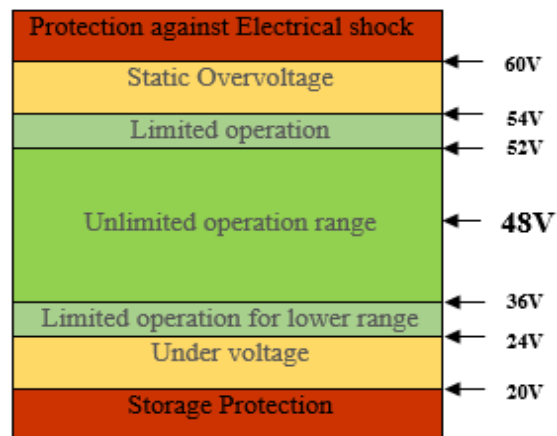


Figure 2.3: VDA 320 standard for 48 V

2.2 Battery Terminologies

A **Battery Pack** consist of individual battery cells connected in series, parallel or mixture of both in order to reach target values of voltage, capacity, and power density.

State of charge is the instantaneous charge available in the battery with respect to the maximum charge. SOC is usually measured in relative numbers with 100% being fully charged and 0% being fully discharged.

Battery Capacity is the maximum amount of charge that can be stored in the battery. Battery capacity is measured in Ampere-hour (Ah) or kilowatt-hour (kWh).

Terminal Voltage is the voltage measured at the output terminal of the battery. Terminal voltage depends on the SOC, temperature, internal resistance and current.

Cut off voltage is the minimum voltage at which the battery is fully discharged and further discharge below this voltage will damage the battery.

C-Rate is the rate at which the battery is charged or discharged relative to its capacity. And it is defined as the charge or discharge current divided by the battery's capacity.

Open Circuit Voltage is the voltage across the cell terminals when no external load is connected and the battery has been electrically rested for a while. The OCV is a static function of the cell SOC and temperature.

Constant current/constant voltage charging (CC/CV): At low SOC the batteries are charged with constant current lower than the maximum charging current. When the maximum charging voltage is reached, the voltage is held constant at this

level and the current is reduced until the battery is fully charged. Figure 2.4 shows CC/CV-charging and discharging procedure.

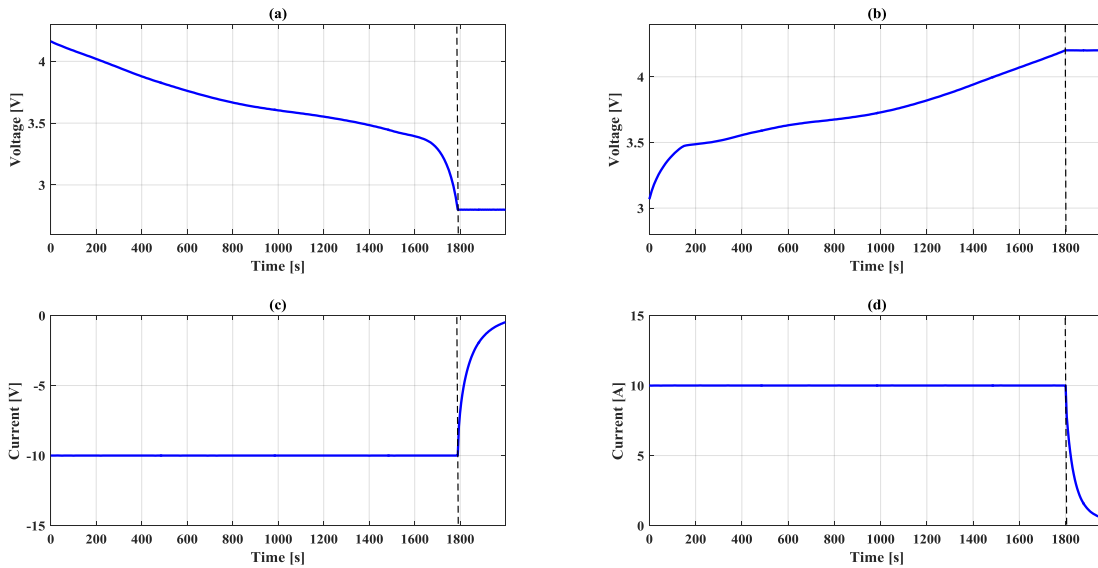


Figure 2.4: (a) Discharge Voltage (b) Charge Voltage (c) Discharge Current (d) Charge Current

2.3 Battery modeling

Depending on the application of a battery model, a trade-off between model complexity and model accuracy has to be done. Too accurate and complex models causes excessive simulation time.

Ideal models can be used when the accuracy of the battery model is not of importance. An ideal battery can be represented as an ideal voltage source with unlimited capacity.

Equivalent Circuit Models (ECM) are used to describe the electrical characteristic of the battery cell. The model is built up with electrical components such as resistances, capacitances and inductances. Model parameters for the ECMs are obtained from either measurements or from physical based models. ECMs usually performs well if the laboratory environment and the test procedures is similar to the environment that the cell is being used in. However, the models can suffer high inaccuracies if the cells are used in vastly different environment and conditions compare to the laboratory environment. Usually the ECMs are very easily connected to other parts of the electrical systems and the control system of the electrical vehicles [16]. Equivalent Circuit Models will be discussed more in depth in the next chapter.

Electrochemical models can be very complex and difficult to formulate. However the electrochemical models, when compared to equivalent circuit models, features

more accurate estimates over larger range of operation conditions. These models can be used to predict aging and degradation phenomena of batteries, and to formulate battery-control algorithms in order to minimize the aging of the battery [17].

2.4 Voltage response to discharge pulse

Polarization voltage is the difference between the open circuit voltage and the cell terminal voltage that appears when the current is flowing through the battery. Figure 2.5 shows a typical voltage response to a discharge pulse of a battery. At the instant when current starts to flow, an instantaneous ohmic voltage drop appears due to the equivalent series resistance in the cell. However, another phenomena can also be observed from figure 2.5 that is the polarization voltage continues to slowly develop as current is drawn from the battery and slowly decays as the battery reaches the rest condition. These processes are caused by slow diffusion processes in the lithium-ion cell [17].

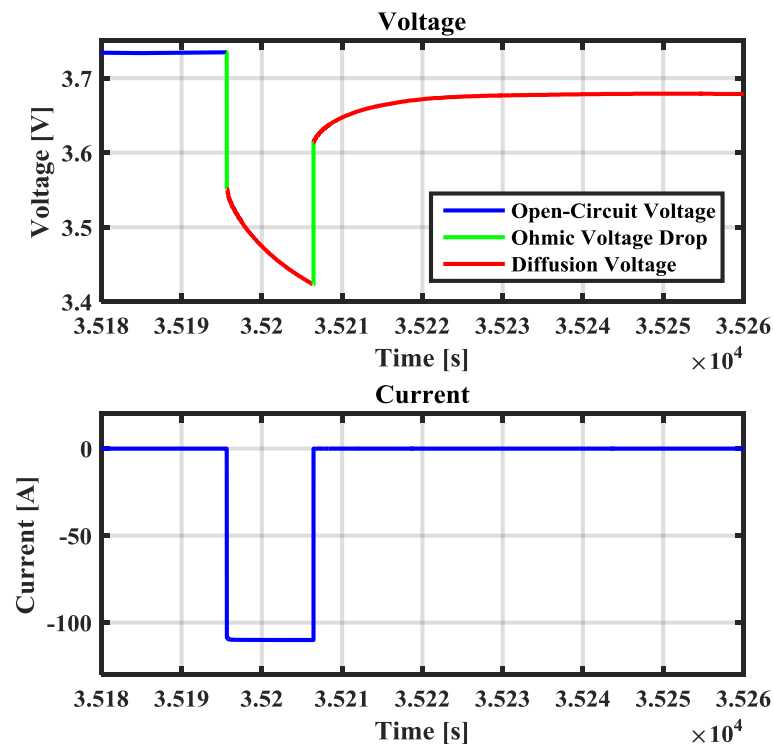


Figure 2.5: Upper: Voltage response, Lower: Discharge current.

2.5 Equivalent-Circuit Models

In this chapter various equivalent circuit models of batteries will be presented. Starting from a simple battery model which can only capture instantaneous polarization and then moving towards more complex models that can capture diffusion voltage is observed in figure 2.5.

2.5.1 Ideal voltage source

Figure 2.6 shows the simplest way to model a battery cell. An ideal battery cell is represented as an ideal voltage source with unlimited capacity. This is rather a poor model of the battery cell. Figure 2.5 clearly shows that the voltage will not remain constant when there is a load current. The terminal voltage depends on factors such as SOC, temperature, load current among other factors [17].

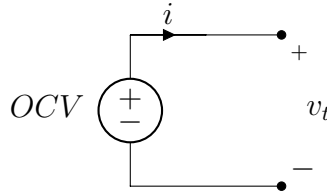


Figure 2.6: Ideal Equivalent Circuit Model of a battery cell

2.5.2 0RC model

The instantaneous voltage drop in figure 2.5 can be modeled with a lumped equivalent series resistance R_0 . The R_0 resistance represents the ohmic losses in the cell and will mainly be a function of SOC and temperature [17]. The model in figure 2.7 can be used for fast computation when good accuracy and dynamic behaviour is not of interest. This model is usually referred as the simple battery model or the zero RC circuit model, also known as a Thevenin equivalent circuit in general electrical engineering circuits.

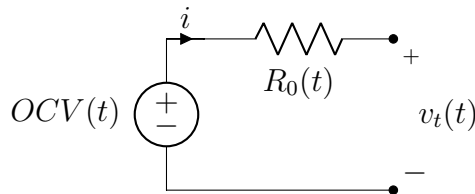


Figure 2.7: 0RC model of a battery cell

The total voltage drop due to the equivalent circuit resistance can be expressed as

$$v_0 = iR_0 \quad (2.1)$$

The terminal voltage is then expressed as

$$v_t = OCV - v_0 \quad (2.2)$$

2.5.3 1RC model

The slow diffusion process can be modeled by introducing RC-links as shown in figure 2.8. If the time constant of the RC-link is chosen to be around 10 s, it will capture fairly fast voltage changes. If instead the time constant is selected in millisecond range, it will capture charge transfer behavior [18].

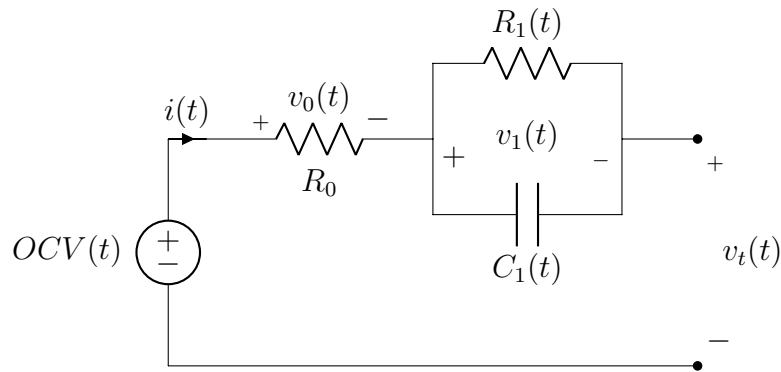


Figure 2.8: Single RC model

The voltage drop over the RC-link can be expressed as

$$v_1 = \int \left(\frac{i}{C_1} - \frac{v_1}{C_1 R_1} \right) dt \quad (2.3)$$

The terminal cell voltage, v_t is then obtained by

$$v_t = OCV - v_0 - v_1 \quad (2.4)$$

2.5.4 2RC model

For long driving cycles with large movements in SOC, the estimating error could be reduced by introducing an additional RC-link with a slower time constant [17]. In [18] the RMSE of the terminal voltage estimation was reduced from 26.25 mV to 10.65 mV by introducing an additional RC link. Figure 2.9 shows the circuit diagram of 2RC model. The concept of RMSE is further explained in section 2.10.

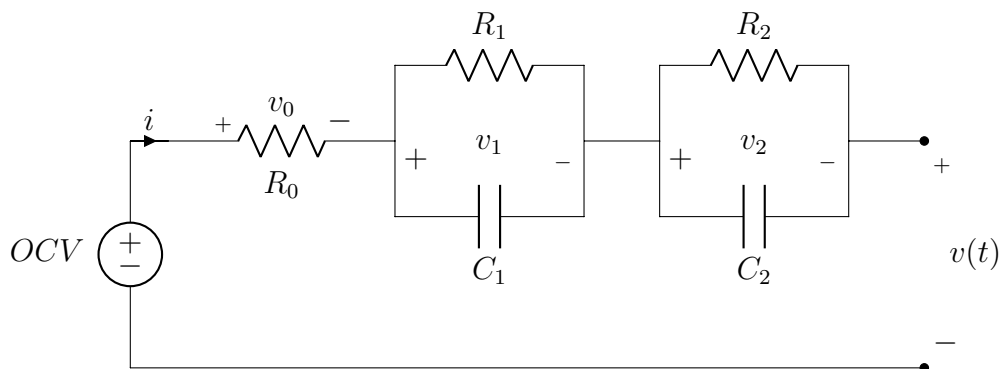


Figure 2.9: Two RC model

The voltage across the 2nd RC link can be expressed as

$$v_2 = \int \left(\frac{i}{C_2} - \frac{v_2}{C_2 R_2} \right) dt \quad (2.5)$$

which is a form that can easily be implemented in Simulink simulation environment. The terminal cell voltage, v_t is obtained by

$$v_t = OCV - v_0 - v_1 - v_2 \quad (2.6)$$

2.6 Electrical model parameter extraction

The RC-link parameters can be extracted either during the discharging or relaxation of the voltage response by making a curve fit. However, since the SOC is constant during the relaxation it is more convenient to extract the parameters during this part of the voltage response. Figure 2.10 highlights the relaxation voltage that is present after a discharge pulse. The procedure used to extract model parameters from the relaxation pulse by performing an exponential curve fit is proposed in [18].

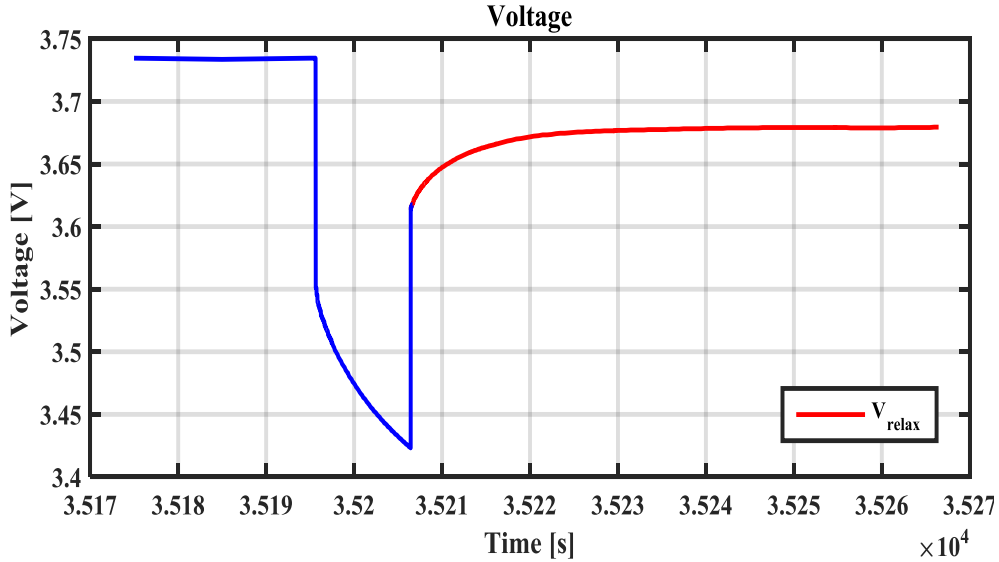


Figure 2.10: Relaxation voltage used for curve fitting

To extract model parameters for a 2RC circuit, a double exponential curve fit is used. The double exponential curve fit can be expressed as

$$V_{relax} = a_0 + a_1 e^{(-b_1 t)} + a_2 e^{(-b_2 t)} \quad (2.7)$$

where a_0 is the steady state voltage after the relaxation, a_1 and a_2 is the maximum polarization voltage at $t = t_0$. The time constant for the RC-links are extracted as

$$\tau_x = \frac{1}{b_x} \quad (2.8)$$

The resistance parameters can be extracted by using the following equation.

$$R_x = \frac{a_x}{i(1 - e^{b_x t_{ch}})}, \quad (2.9)$$

where t_{ch} is the length of the discharge pulse and i is the discharge current. The capacitance values for the RC links can be extracted according to,

$$C_x = \frac{\tau_x}{R_x} \quad (2.10)$$

The parameters are grouped with the SOC value at which the relaxation begins. To extract model parameters for 1RC model instead, a single exponential curve fit should be used.

Other equivalent resistances of interest are 2, 10 and 30-second resistances, denoted as the R_{2s} , R_{10s} and R_{30s} resistances, which can be extracted according to,

$$R_{xs} = R_0 + R_1 e^{\left(\frac{-t_x}{\tau_1}\right)} + R_2 e^{\left(\frac{-t_x}{\tau_2}\right)} \quad (2.11)$$

where R_{xs} corresponds to the resistance at 2, 10 and 30-second after the discharge pulse appear. Figure 2.11 shows where the R_{2s} , R_{10s} and R_{30s} are extracted during a discharge pulse.

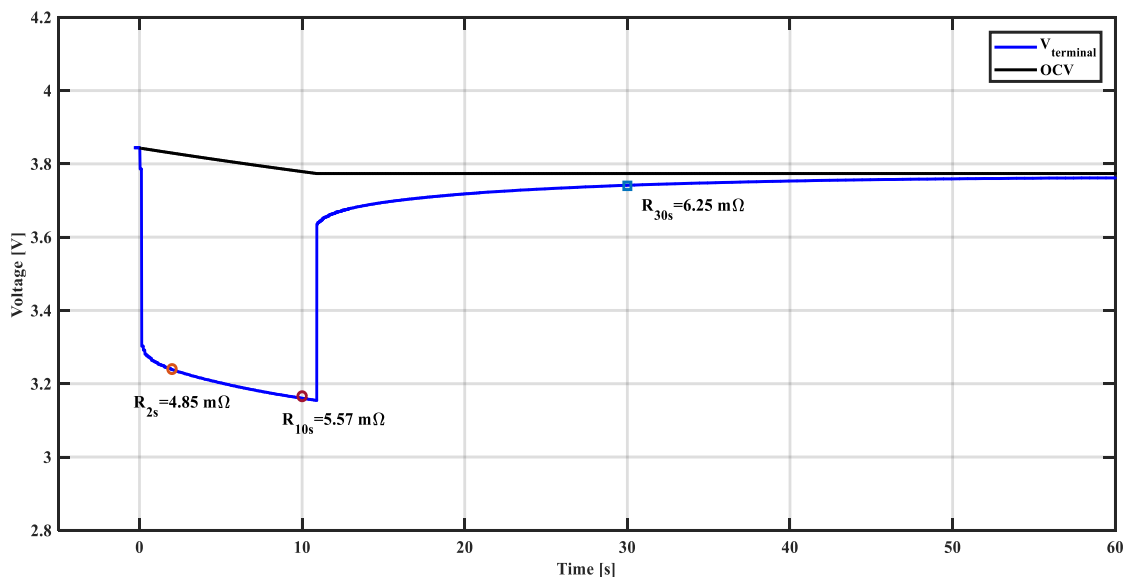


Figure 2.11: Visualization of where the R_{2s} , R_{10s} and R_{30s} are extracted during a discharge pulse

2.7 State of Charge estimation

The state of charge of a battery cell can be described with an ordinary differential equation according to

$$\frac{d(SOC(t))}{dt} = \frac{\eta(t)i(t)}{Q_{max}} \quad (2.12)$$

where $\eta(t)$ is a charge efficiency, $i(t)$ is the cell current [A] and Q_{max} is the total charge capacity of the cell [Ah]. When a cell is charged, not all the charge that passes through the cell participates in the chemical reactions which increases the

state of charge therefore, $\eta(t) \leq 1$ [17]. The charge efficiency of the cell is dependent on SOC, temperature and charging rate among other things, hence it can be difficult to model accurately. Li-Ion batteries generally have high charge efficiency, typically around 99% therefore $\eta(t)$ can usually be neglected [20]. Integrating (2.12) knowing the initial SOC yields

$$SOC(t) = SOC_0 - \frac{\int_{t_0}^t \eta(t) \cdot i(t) dt}{Q_{max}} \quad (2.13)$$

where SOC_0 is the state of charge at time t_0 .

2.8 48 V Battery pack

A single Li-ion cell can only supply a certain amount of voltage and capacity. Therefore batteries which are intended for electric vehicle application consist of several cells connected in series and parallel in order to meet target values of voltage and capacity. Figure 2.12 shows an equivalent circuit diagram of a 48 V battery pack. The battery pack has a 12 cell pairs connected in series (12s2p cell configuration) and also includes a connection between cells, fuse, a relay and a battery management system (BMS). Due to parasitic elements, resistive losses will occur between the cell pairs as well as due to the resistance of the connections, relay, fuse and BMS. The fuse provides overcurrent protection of the battery pack. The relay works as a switch, when the relay is open, the battery pack is disconnected from the 48 V electrical system. The BMS manages the 48 V battery pack and protects the battery from operating outside its safe operating area (SOA). The BMS monitors voltage, current and temperature in order to optimize the battery pack performance.

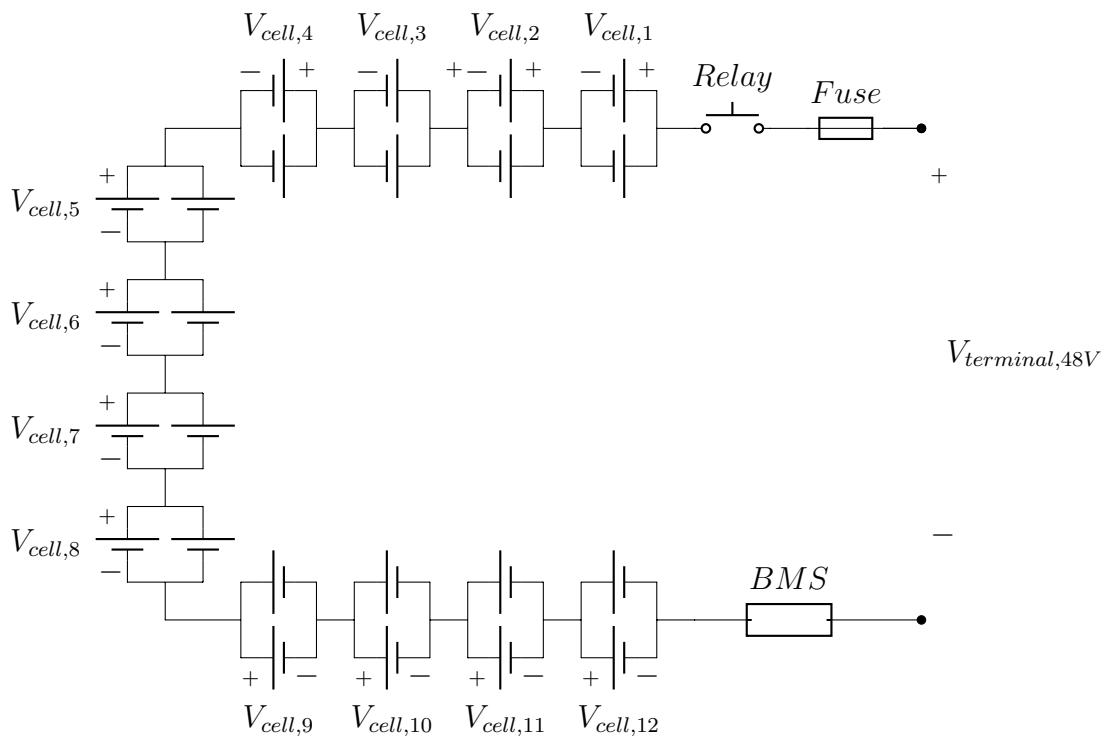


Figure 2.12: Electrical Circuit diagram of a 48 V battery pack with 12s2p cell configuration

2.9 Temperature Modeling

Heat transfer occurs due to spatial temperature differences and is classified into three different transfer mechanisms: thermal conduction, thermal convection and thermal radiation. Thermal conduction is the mechanisms in which heat is transferred in a solid medium, for example through the housing of a battery pack. Thermal conduction is describe by Fourier's law according to

$$Q_{Conductive} = kA \frac{dT}{dx}, \quad (2.14)$$

where k is the thermal conductivity of the material in $[\frac{W}{mK}]$, A is the area normal to the heat flow direction in $[m^2]$ and, $\frac{dT}{dx}$ is the temperature gradient in $[\frac{K}{m}]$. When the temperature distribution is linear, the equation can be rewritten to the following form

$$Q_{Conductive} = kA \frac{\Delta T}{D}, \quad (2.15)$$

where D is the thickness of the material in $[m]$ and ΔT is the temperature difference between the two sides of the material in $[K]$.

Thermal convection is the transfer of heat from one place to another by the movement of fluids, for example air inside the battery pack. Thermal convection can be

divided in to free convection or forced convection. Thermal convection is described by Newton's law of cooling according to

$$Q_{Convective} = hA(T - T_{amb}) \quad (2.16)$$

where h is the convection heat transfer coefficient in $[\frac{W}{m^2K}]$, A is the surface area in $[m^2]$, T is the temperature of the source in [K] and T_{amb} is the fluid temperature [K].

Another important concept is the thermal mass of an object which is the ability of a material to store internal energy and provide inertia against temperature fluctuations. The equation relating thermal energy to thermal mass is described as,

$$Q = mc_p \frac{dT}{dt} \quad (2.17)$$

where c_p is the specific heat capacity $[\frac{J}{K}]$, m is the mass of the body [kg], and $\frac{dT}{dt}$ is the instantaneous change in temperature in $[\frac{K}{s}]$. The mc_p -product is referred to as thermal mass of the body [25].

2.9.1 1D lumped-parameter method

The simplest method of modeling the heat transfer between a cell and its environment is with a 1D lumped-parameter model which can be described as

$$Q = mc_p \frac{dT}{dt} + hA(T - T_{amb}) \quad (2.18)$$

where Q is the rate of heat generation by the cell [W], T is the cell temperature [K], T_{amb} is the ambient temperature [K], h is the heat transfer coefficient including both convection and conduction effects $[\frac{W}{m^2K}]$, and A is the equivalent heat transfer area $[m^2]$. In the 1D lumped-parameter model, the radiation is neglected since the thermal difference between the cells and ambient temperature is typically low [21]. The heat generated by the cell can be expressed as

$$Q_{joule} = (ocv - v_t)i \quad (2.19)$$

where Q_{joule} is joule heat [W], which is the irreversible heat that is generated by the cell.

2.10 Root-Mean-Square Error (RMSE)

The RMSE is the sample standard deviation of the differences between predicted values for example from simulations and an observed values from a laboratory test [26]. The RMSE voltage is used to quantify model accuracy in this report. The estimated error E can be expressed as,

$$E = \hat{v} - v \quad (2.20)$$

where \hat{v} is the simulated value, v is the measured value. The RMSE is then defined as

$$RMSE = \sqrt{\frac{1}{n} \sum_{t=1}^n E^2} \quad (2.21)$$

where n is the number of measurement points.

2.11 WLTP

The Worldwide Harmonised Light Vehicle Test Procedure (WLTP) driving cycle is the new test cycle developed on the basis of actual driving data obtained around the world. It covers everyday driving scenarios from heavy urban traffic, rural driving to highway driving. This was developed and accepted as standard global driving cycle as fuel consumption, $C0_2$ emission as well as pollutants can be compared worldwide. The driving cycle was divided into four levels based on the speed: low, medium, high and extra high. In addition to this, each level has various phases such as stop, acceleration, braking phases [22].

3

Method

This thesis work was organized in five defined steps. Each step was conducted successively. The comprised steps are listed below and each will be further explained later in the following sections.

1. Extract electrical model parameters for three high-performance li-ion cells using the available raw measurement data.
2. Develop single cell electrical models (0RC, 1RC and 2RC models) and compare the models in terms of accuracy and efficiency.
3. Extend the cell models to battery pack models. Verify the models in terms of accuracy by comparing them with measurement data and reference model provided by VCC.
4. Extend the electrical battery pack models to include thermal losses and temperature effects. Verify the thermal model comparing them with measurement data provided by VCC.
5. Perform 48 V system simulation including an ISGM model and a 48 V battery pack model.

3.1 Extracting electrical model parameters

The Raw measurement data has been acquired from cell test performed at the division of Electric Power Engineering at Chalmers, using the same methodology as explained in [18]. The raw data was used to extract the electrical model parameters for the 0RC,1RC and 2RC models discussed in section 2.5. Three different high-performance Li-ion cells were tested with the methodology explained in [18]. The cells are tested over a temperature range between -10 °C and 60 °C. The test is based on high-current discharge pulses with well-defined pulse lengths and depths. The method is suited for analysis of electrical time dynamics from 0.3 mHz to 10 Hz, focusing mainly on diffusion voltage caused by electrochemical mass transport. The cells are referred to as 'N1', 'M1' and 'T3' in this report according to Stefan Skoog's lab designations. Table 3.1 shows the cells that has been evaluated

Table 3.1: The cell characteristics obtained from datasheets

Nickname	Form Factor	Chemistry	Capacity [Ah]	Nominal [V]	Upper cut-off [V]	Lower cut-off [V]
N1	Pouch	NMC/LTO	11	2.2	2.7	1.5
M1	Prismatic	NMC/G	5	3.86	4.2	2.8
T3	Prismatic	LMO/LTO	11.5	2.45	2.7	1.8

3.1.1 Laboratory tests

The test consist of a capacity test and a discharge pulse test. The test procedure is explained below

1. The cell is installed in a cell holder and electrically connected to the battery test system Digatron BTS-500.
2. The set up is placed in a climate chamber and rested until thermal equilibrium is achieved.
3. Capacity test
 - (a) The cell is charged to max voltage with CC/CV procedure, then the cell rested for 30 to 60 minutes.
 - (b) The cell is fully discharged with CC/CV procedure.
 - (c) The cell is fully recharged with CC/CV procedure.
 - (d) The cell is put in relaxation during 30 to 60 minutes.
4. Discharge Test
 - (a) Pulse discharging is performed by applying 10-16 pulses at 5C for the 'N1' and 'T3' cells. The 2C discharge rate is used for cell 'M1'. Each pulse needs 30-60 min of relaxation.
 - (b) After the last pulse measure the remaining cell capacity is measured through 2C discharge.
5. Repeat procedure from (3) for a new test temperature.

Figure 3.1 shows the raw data from a capacity test of the 'M1' cell at 25 °C. This data together with the data from the other test temperatures can be used to extract the capacity of the battery as a function of temperature.

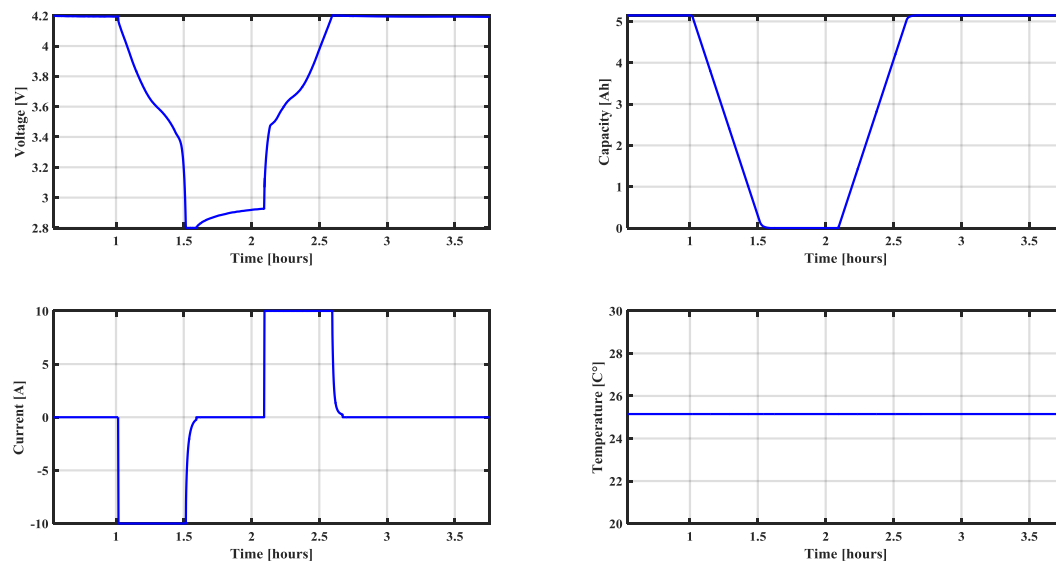


Figure 3.1: Capacity test of cell 'M1' at 25 °C

Figure 3.2 shows the raw data from a complete discharge test as well as a zoom of a single discharge pulse of the 'M1' cell at 25 °C. The zoom of the voltage response clearly shows the instantaneous voltage drop as well as the diffusion voltage during discharge and relaxation time, which was discussed in section 2.4. For each discharge pulse the electrical parameters OCV, R_0 , R_1 , C_1 , R_2 , C_2 can be extracted by making a curve fit on the relaxation part of the voltage response as discussed in section 2.4

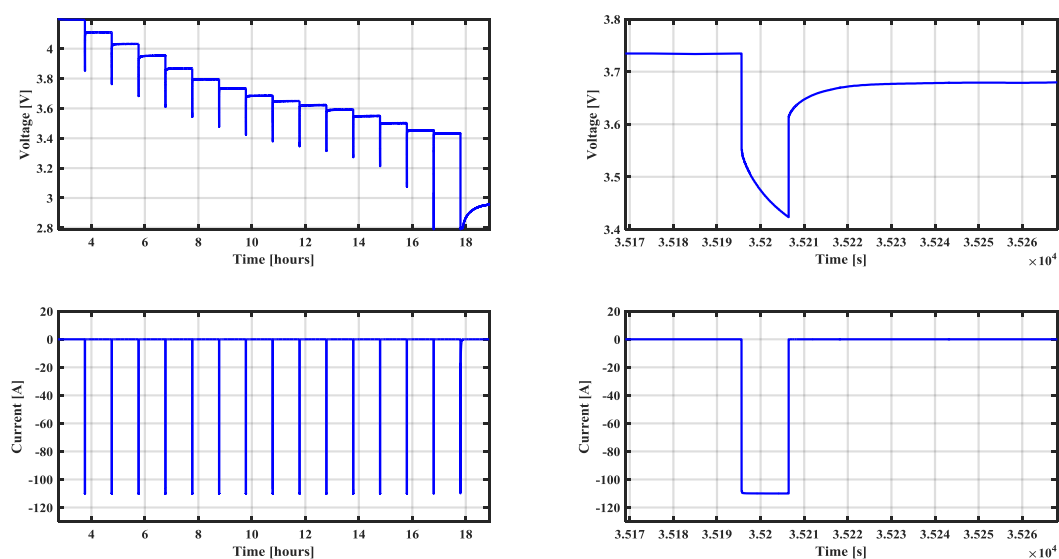


Figure 3.2: Discharge pulse test of cell 'M1' at 25 °C

3.1.2 Curve Fitting

To be able to analyze the pulses individually, a script that detects transients in the raw data and cuts all discharge pulses into individual pieces are utilized. Figure 3.3 shows the results of a successful voltage transient detection.

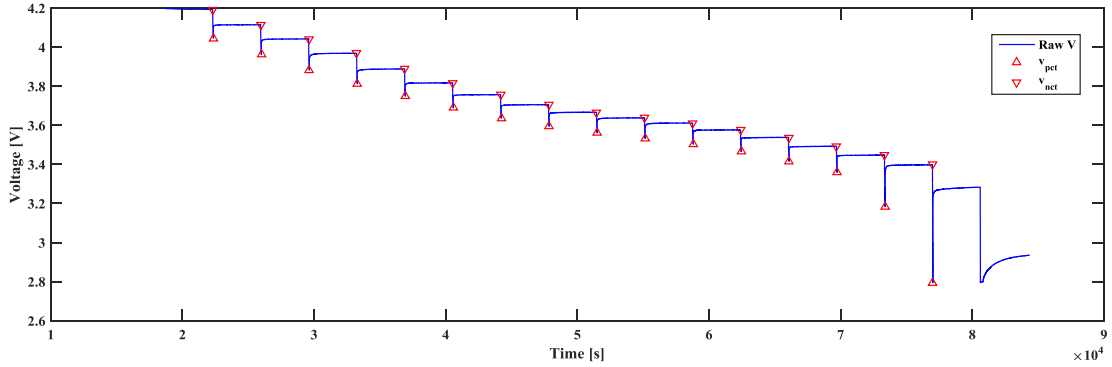


Figure 3.3: Raw voltage together with detected positive and negative transients

Figure 3.4 shows relaxation voltage together with the exponential curve fits. Knowing the discharge current and the time length of the discharge pulse, the RC parameters can be calculated with (2.8), (2.9) and (2.10). All parameters are stored together with the SOC and temperature. The equivalent values for R_{2s} , R_{10s} and R_{30s} are also calculated and stored.

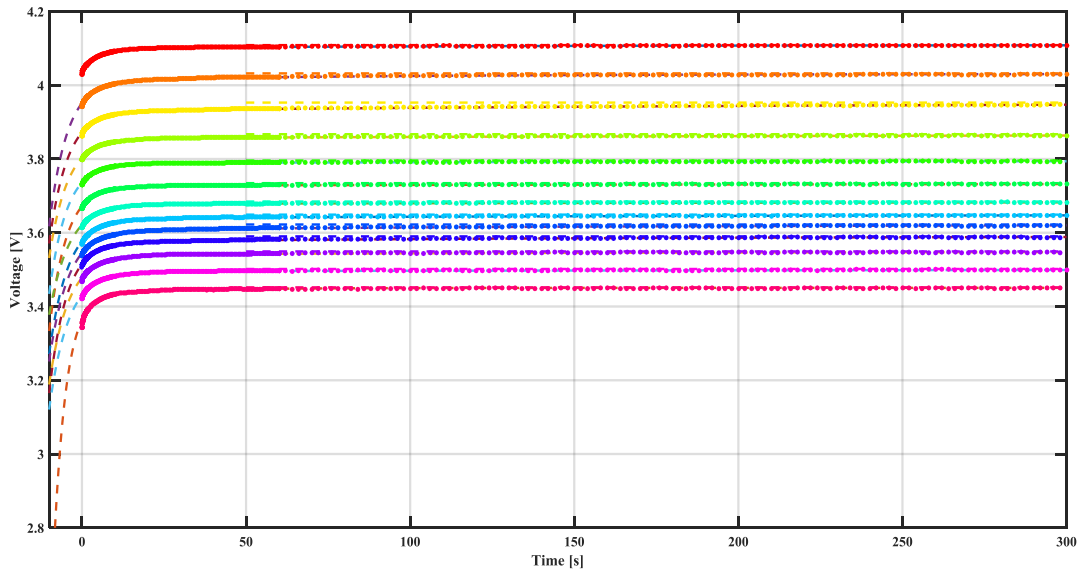


Figure 3.4: Extracted relaxation voltage from each pulse in and their exponential curve fit

In order for the battery model to support continuous SOC between 0% and 100%, the parameters are linearly interpolated with steps of 1%. For SOC levels higher

than the first relaxation voltage and lower than the last relaxation voltage (roughly 10% and 90%), the model parameters are kept constant at the last measurement point which can be observed in figure 3.5.

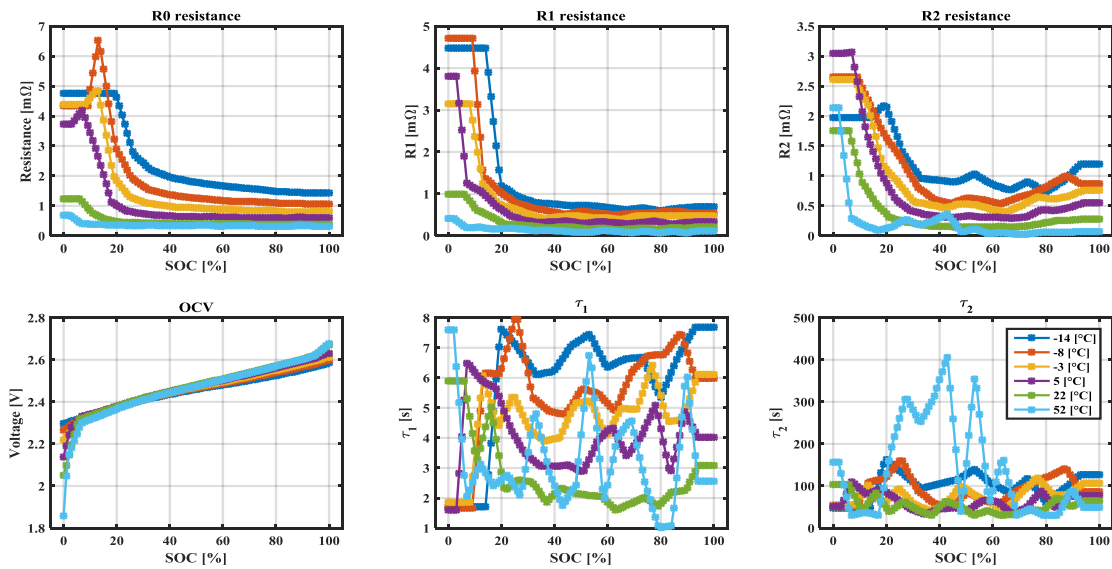


Figure 3.5: 2RC parameters of cell 'T3' linearly interpolated

In order to support continuous temperature range between $-10\text{ }^{\circ}\text{C}$ and $60\text{ }^{\circ}\text{C}$ the model parameters from different test temperatures (-10 , -5 , 0 , 8 , 25 and $60\text{ }^{\circ}\text{C}$) are linearly interpolated in the same way as the SOC. Figure 3.6 shows the surface plots of the linearly interpolated 2RC model parameters. The parameters matrices can be implemented in Simulink 2D look-up tables together with the SOC and temperature range.

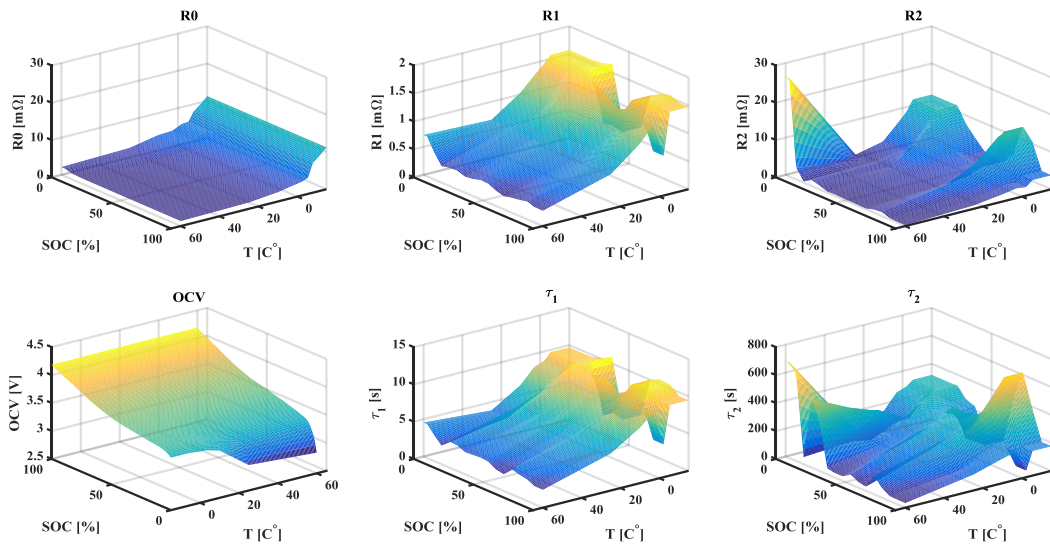


Figure 3.6: 2RC model parameters for cell M1

3.2 Component model implementation in Simulink

This section describes the electrical battery cell model, electrical battery pack model as well as the electro-thermal battery pack model implementation in Simulink.

3.2.1 Electrical cell model

Figure 3.7 shows the electrical model of the 2RC model as implemented in Matlab Simulink. This model was implemented to verify the model parameters extracted from the curve fitting of the relaxation pulses. The input variables given to this model are initial SOC, temperature and current profile from the discharge pulse test raw data.

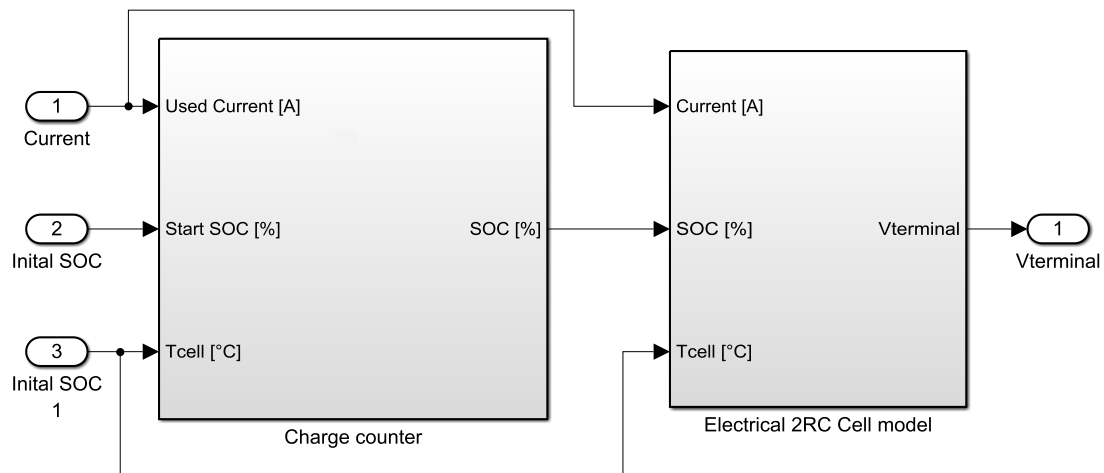


Figure 3.7: Electrical model of the battery cell

Figure 3.8 shows the charge counter that is implemented to calculate the instantaneous SOC according to (2.13). A 1D look up table is implemented for the cell capacity because of its strong temperature dependency.

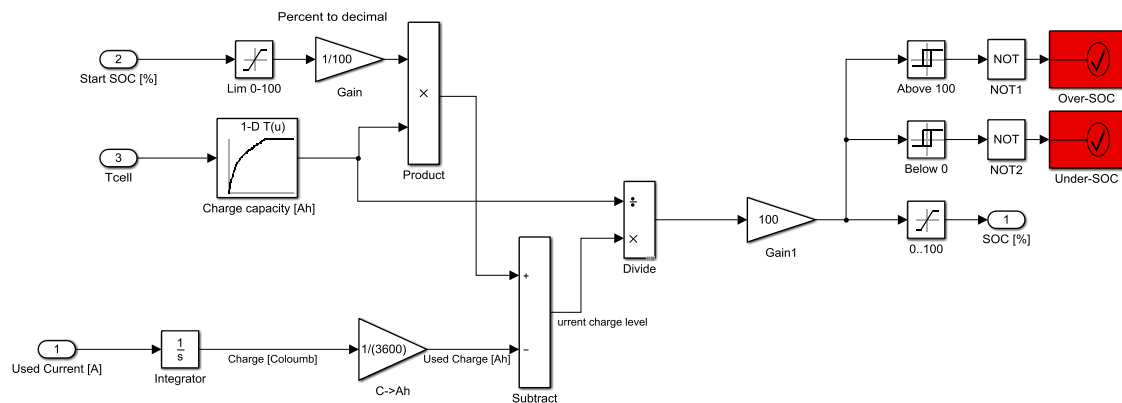


Figure 3.8: Charge Counter used to calculate SOC level

Figure 3.9 shows the electrical 2RC model implementation in Simulink. The 0RC, 1RC and 2RC blocks are implemented by using (2.1), (2.3) and (2.5). The look up table block contains 2D data for each of the model parameters in figure 3.6.

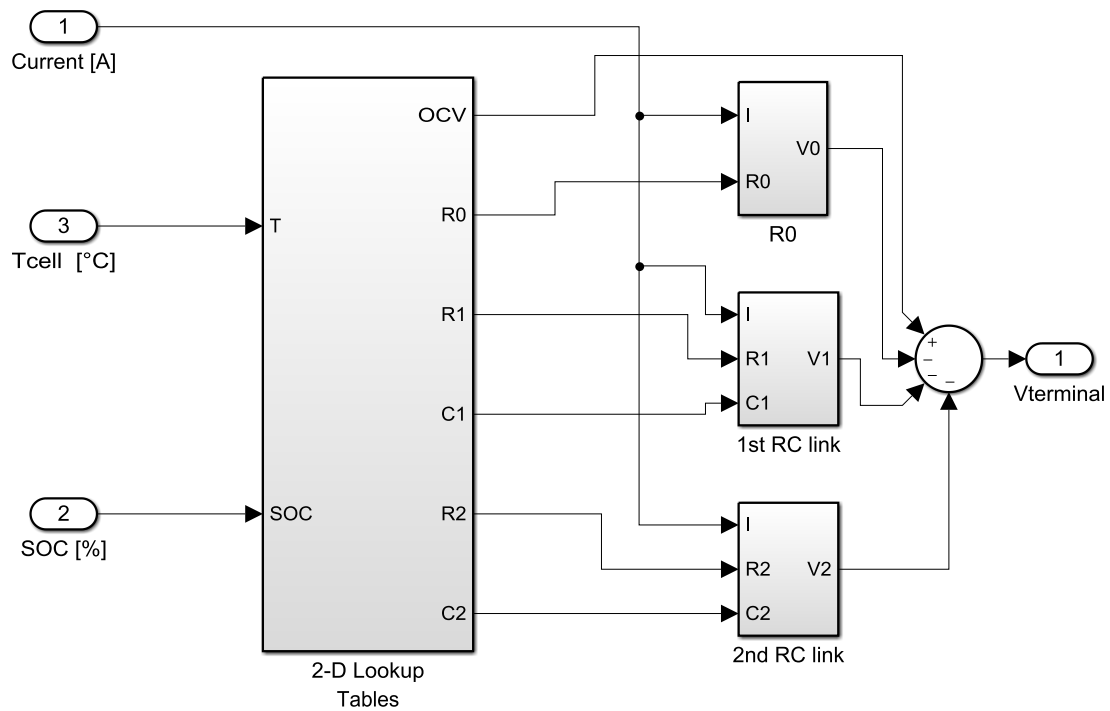


Figure 3.9: 2RC Electrical Cell model

Figure 3.10 was implemented according to (2.3) in Simulink, in order to calculate the voltage drop over the RC links.

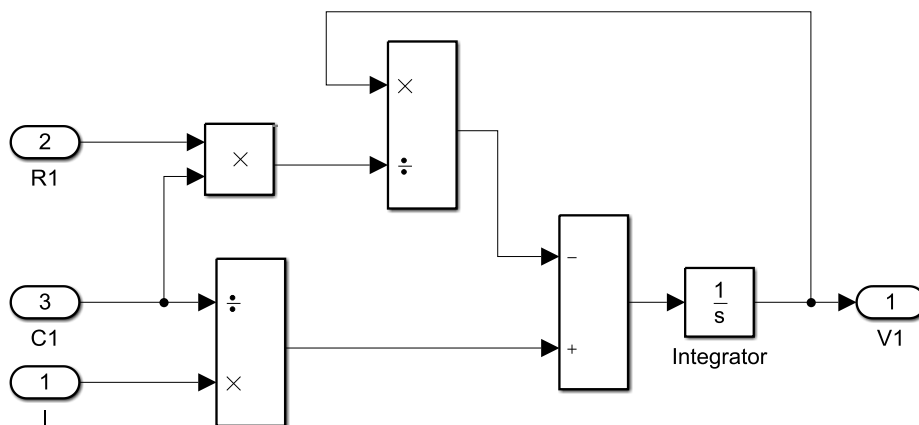


Figure 3.10: RC link block implementation

3.2.2 Electrical Battery Pack Model

Figure 3.11 shows the parallel cell implementation in Simulink. Since the 48 V battery pack has a 12s2p cell configuration, the resistance has to be divided by 2

and the capacitance has to be multiplied by 2 in order for the time constant to remain the same.

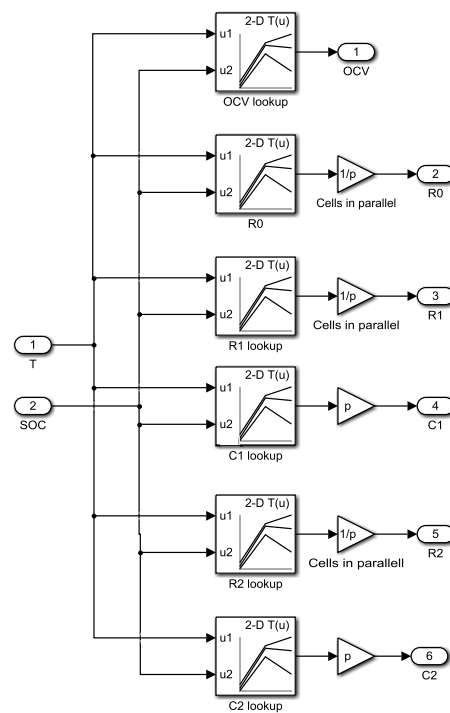


Figure 3.11: Implementation of parallel cells in Simulink

Since the battery pack has a 12s2p cell configuration, the output of the electrical model has to be multiplied by 12. The difference in individual cell voltage will be neglected since it was discovered that it was insignificant, which can be observed in figure 3.12.

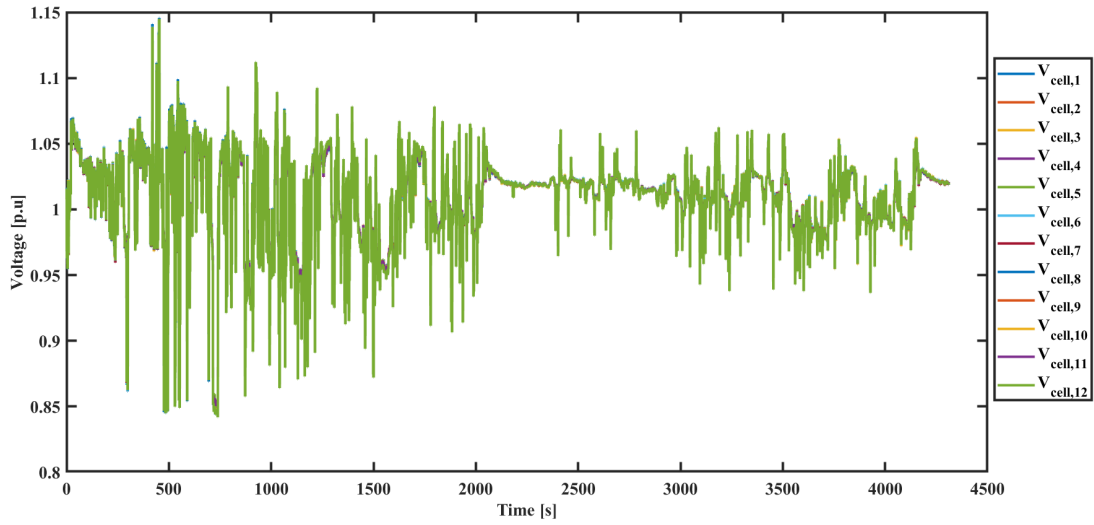


Figure 3.12: Individual cell voltage in p.u for a WLTP cycle

Figure 3.13 shows the electrical model of the 48 V battery pack. The constant s represent the number of cells in series, R_{int} represent the lumped resistance of the fuse, relay, connections between the cells and the current shunt of the BMS. The total R_{int} roughly represent on a one additional cell in terms of resistance, thus $2\text{ m}\Omega$ was chosen, which was close to the R_0 of the 'M1' cell at room temperature.

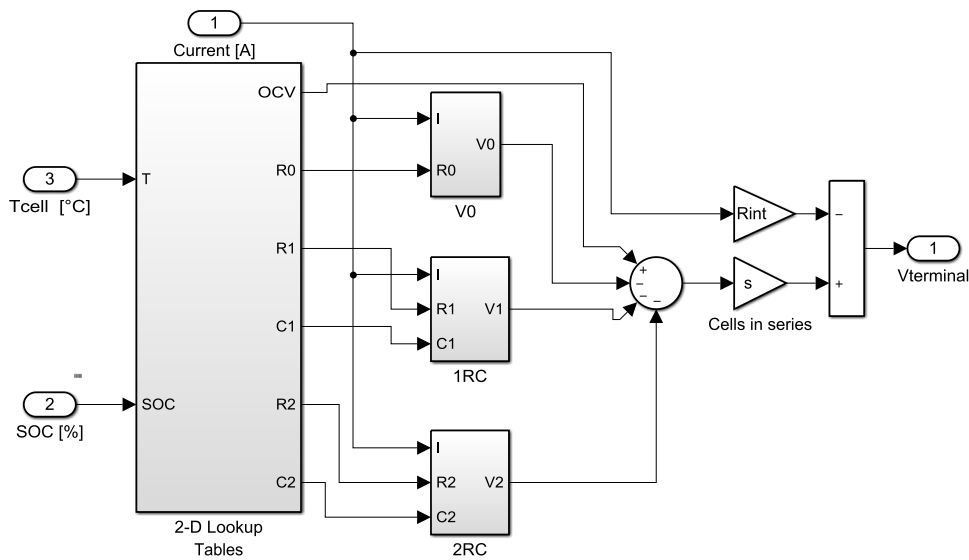


Figure 3.13: 48 V battery pack electrical model

3.2.3 Electro-thermal Cell Model

Figure 3.14 shows the electro-thermal battery pack model. The inputs to the electrical model are initial SOC, current profile and cell temperature. The electrical

model output Q_{heat} is the rate of heat generated by the cells which is fed in to the 1D-lumped parameter model inside the thermal model block. The thermal model block calculates the cell temperature, which is fed back into the electrical model to adjust the total capacity and the model parameters for each iteration.

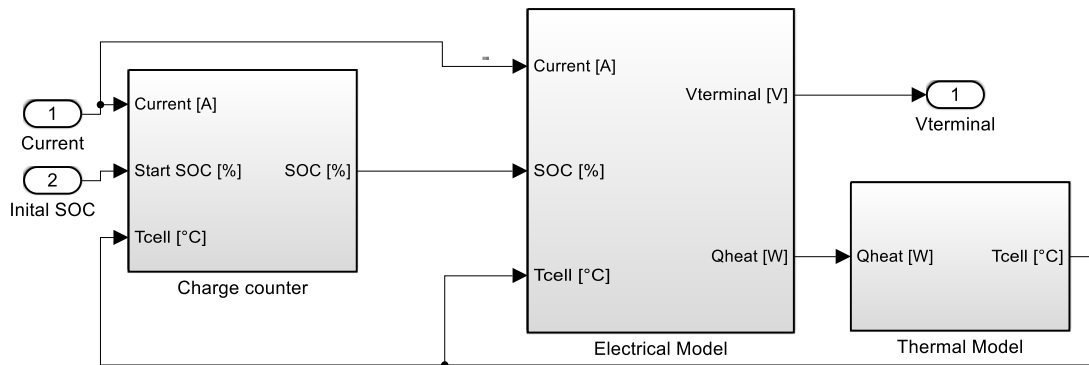


Figure 3.14: Electro-thermal model

Figure 3.15 shows the implementation of 1D-lumped parameter model according to (2.18). The ambient temperature used in this model is from a temperature sensor under the housing of the battery pack. The cells in the battery pack is thermally and mechanically connected to the bottom- and backside of the housing.

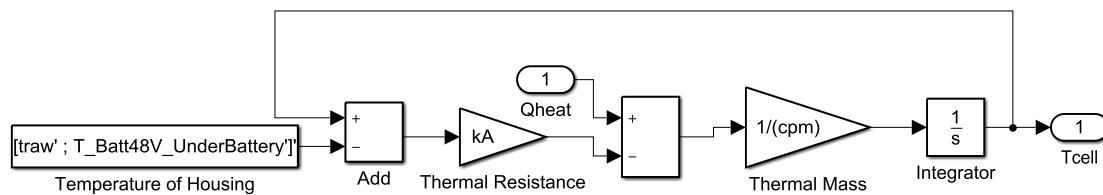


Figure 3.15: 1D-lumped parameter model implementation in Simulink

3.3 48 V system simulation

Figure 3.16 shows the 48 V system simulation setup including a ISGM model and the developed battery pack model. In order to simplify the simulation, the 12 V system and the DC/DC converter is not implemented, instead current measured from the DC/DC converter high side is used as an input to the model. The system is tested with a WLTP driving cycle. The detailed description about the results will be explained in section 4.5.

3. Method

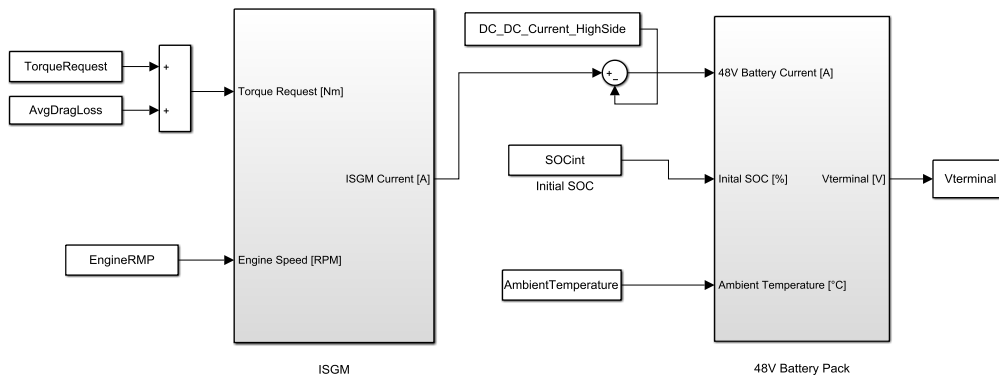


Figure 3.16: 48 V system simulation setup including ISGM and Battery Pack model

4

Results

In the following chapter the results of the study are presented and discussed continuously. Firstly, the parameters extracted from the measurement data of the three different high-performance Li-ion cells are presented and analyzed. Secondly, the 0RC, 1RC and 2RC electrical models are compared in terms of accuracy for each cell. Finally, the developed electro-thermal battery pack model is evaluated in terms of SOC, voltage and temperature estimation.

4.1 Cell Capacity

Figure 4.1 shows the maximum cell capacity as a function of temperature for a constant discharge current. The capacity gradually decreases when the temperature drops below 20°C for all three cells. This is due to retardation of the chemical metabolism which impede the chemical reaction rate [27]. However, for the 'N1' cell the capacity also drops between the 19°C and 57°C measurement, this is something that can be attributed to measurement uncertainty since the capacity is expected to increase for higher temperatures. It can be observed that the capacity of the M1 cell is decreasing much faster between +20°C to -20°C and the T3 cell is retaining most of its capacity among the three cells.

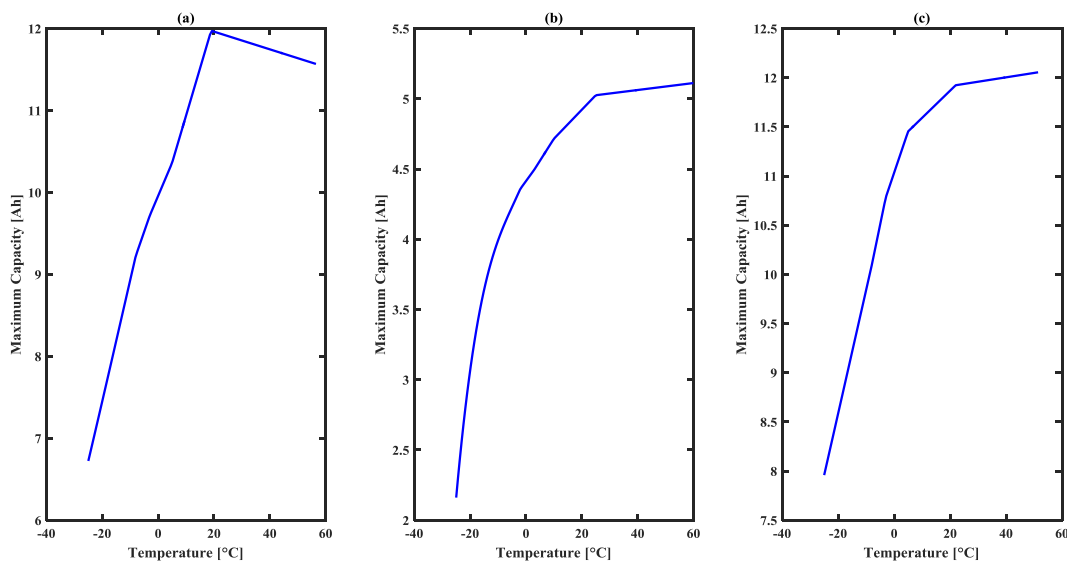


Figure 4.1: Maximum capacity vs temperature (a) 'N1' (b) 'M1' (c) 'T3'

4.2 Equivalent circuit model parameters

This chapter presents the results from the curve fitting of the relaxation pulses discussed in section 3.1.2 . The results include equivalent resistances, time constants and OCV for the three cells.

4.2.1 Equivalent resistance

Figure 4.2 shows the R_0 , R_{2s} , R_{10s} and R_{30s} resistance of the LTO cell 'N1'. It is observed that the resistance is increasing with decreasing temperature, which is expected, due to the fact that reaction rate slows down for lower temperatures and the ion mobility in the electrolyte decreases [28]. It is also observed that the resistance increases significantly for low SOC.

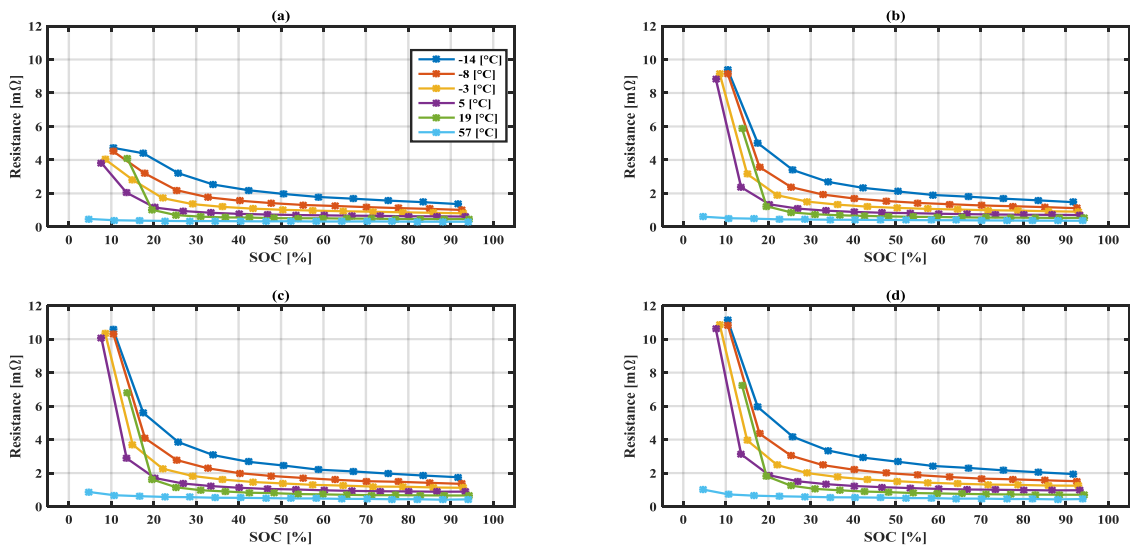


Figure 4.2: R_0 , R_{2s} , R_{10s} and R_{30s} for the cell 'N1'

Figure 4.3 shows the R_0 , R_{2s} , R_{10s} and R_{30s} resistance of the NMC cell 'M1'. It can be observed that the NMC cells' resistance vary less with SOC, compared to the resistance of the LTO cells. However, similar temperature dependence can be observed for different cells.

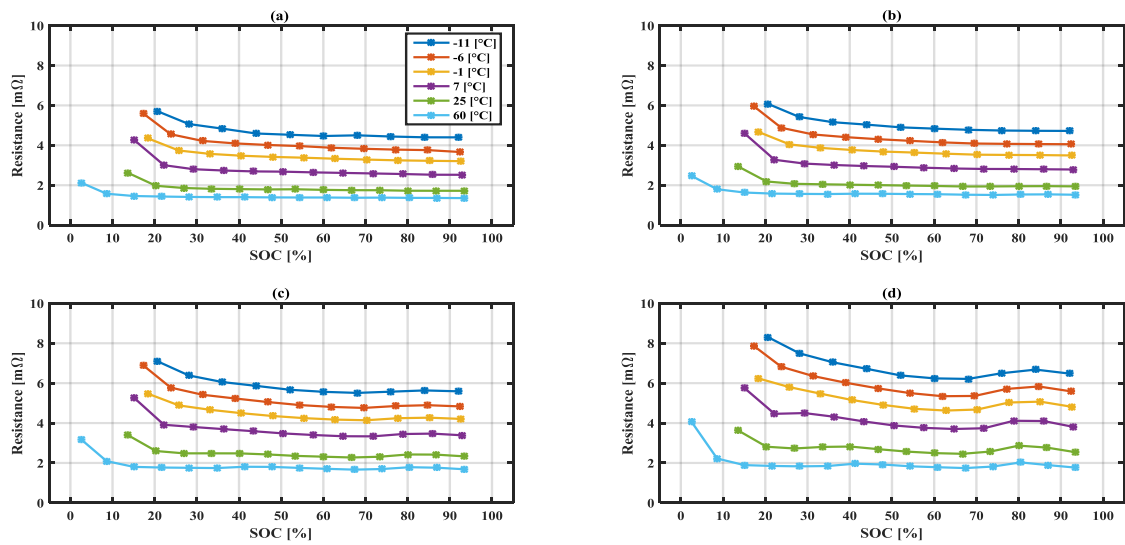


Figure 4.3: R_0 , R_{2s} , R_{10s} and R_{30s} for the cell 'M1'

Figure 4.4 shows the equivalent resistances of the LTO cell 'T3'. It is observed that the difference between the R_{2s} and R_{30s} resistance is much smaller for the LTO cells compared to the NMC cell. This is because LTO have less mass transport and react electrochemically faster compared to the NMC cell.

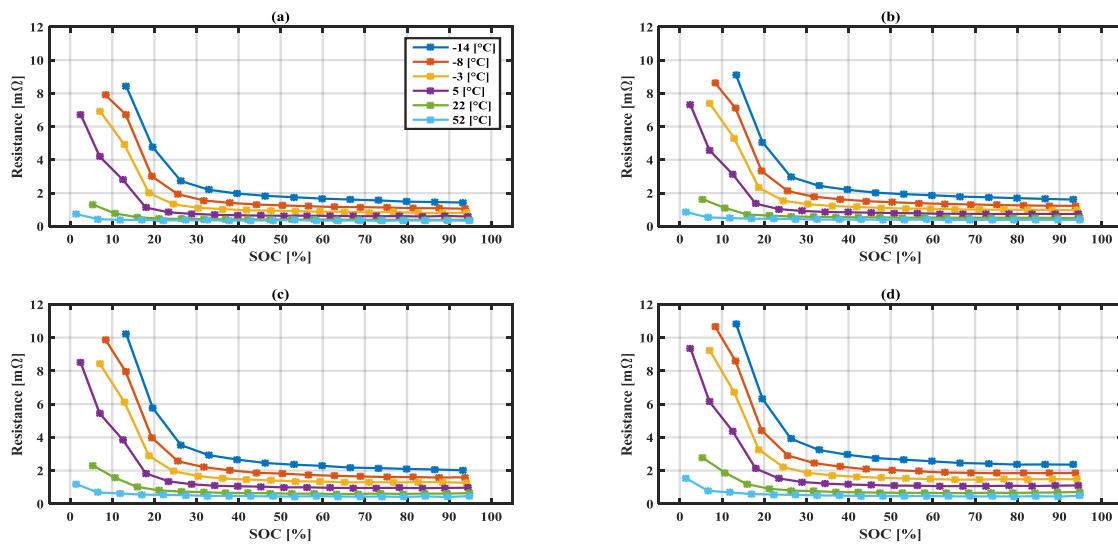


Figure 4.4: R_0 , R_{2s} , R_{10s} and R_{30s} for the cell 'T3'

4.2.2 2RC Model parameters

Figure 4.5, 4.6 and 4.7 show the 2RC model parameters for the 'N1', 'M1' and 'T3' cells respectively. It is observed that the OCV does not change much with

4. Results

temperature between 20% and 90% SOC. However, at higher and lower SOC, the OCV is more temperature sensitive. From the graphs it is observed that at high temperature, the OCV curve has both the highest maximum voltage and the lowest minimum voltage. Something that has to be considered is that at high temperatures, it is much easier to test at very low SOC and therefore it is possible to get measurement points closer to 0% SOC. For low temperatures, some of the tests ends at 10-15% SOC due to high internal resistance. The last OCV point is measured after CC discharging at a lower rate than the default test pulse current. Hence, the low temperature measurement series will not be as reliable as the high temperature measurements for the low SOC.

The R_0 resistance shows a significant increase for low SOC levels for the LTO cells ('N1' and 'T3'), while the NMC cell ('M1') shows a slight increase in resistance for low SOC. As discussed in section 4.2.1, it is expected that the resistance increase with decreasing temperature for all cells due to slower reaction rate.

The fast time constant for the N1 cell does not change significantly between 25% and 100% SOC. However, at lower SOC the time constant is significantly faster compared to medium and high SOC. The reason for the zigzag behaviour in τ_1 and τ_2 parameters are not analyzed in this thesis. It is noted that the time constant increases with a decrease in temperature. In case of the M1 cell, the time constant remains almost constant with SOC. For the LTO cells it is noted that the slow time constant and the R_2 resistance is much lower compared to the NMC cell. This means that the slow time constant, contribute less in OCV estimation and in $I^2 * R$ losses for LTO cell compared to the NMC cell.

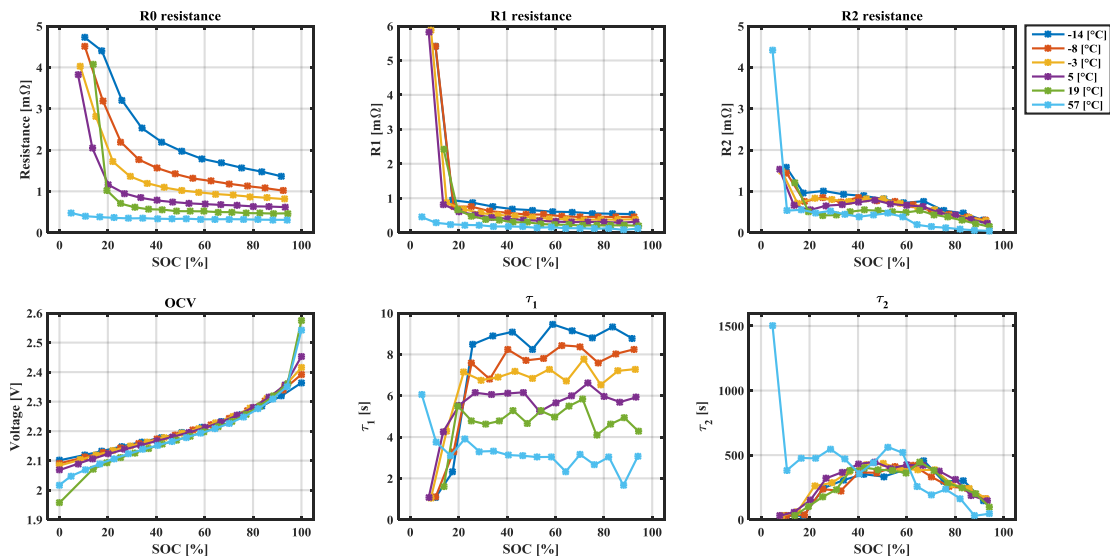


Figure 4.5: 2RC models parameters for cell N1

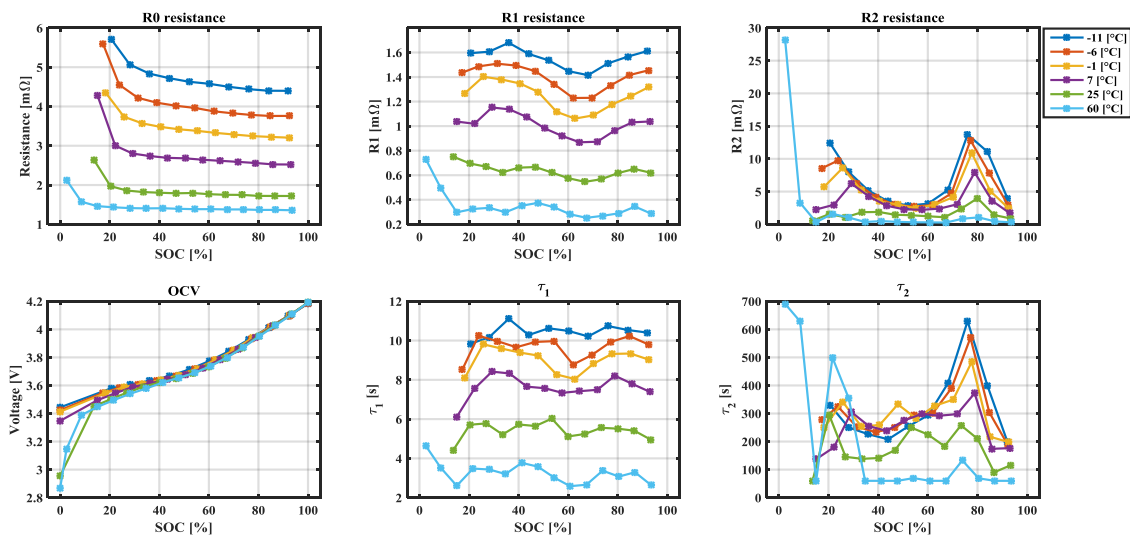


Figure 4.6: 2RC models parameters for cell M1

The R_0 resistance value in figure 4.7 is much lower at higher SOC compared to the other two cells. In this case, more zigzag behaviour is seen as compared to figure 4.5 and 4.6. It can be noted that the τ_2 time constant extracted from the 52° measurements varies more than the other time constants, this is because the LTO cells, such as ‘T3’ cell react electrochemically faster, especially at higher temperatures. Therefore the curve fitting script has trouble finding a slow time constant for those measurements.

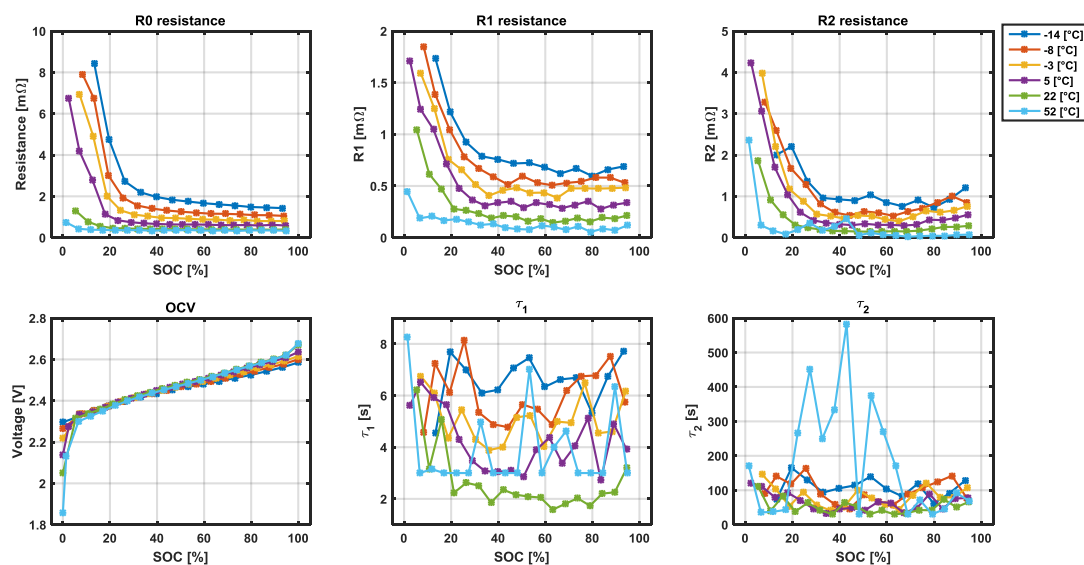


Figure 4.7: 2RC models parameters for cell T3

4.2.3 1RC Model parameters

Figure 4.8 shows the R_1 and τ_1 parameters for all three cells when using the simpler 1RC model. The relationship between R_0 , OCV, R_1 , τ_1 with SOC and temperature works in the similar way as the 2RC model but the difference is that the time constant τ_1 of the 1RC model is higher compared to the τ_1 time constant of the 2RC model.

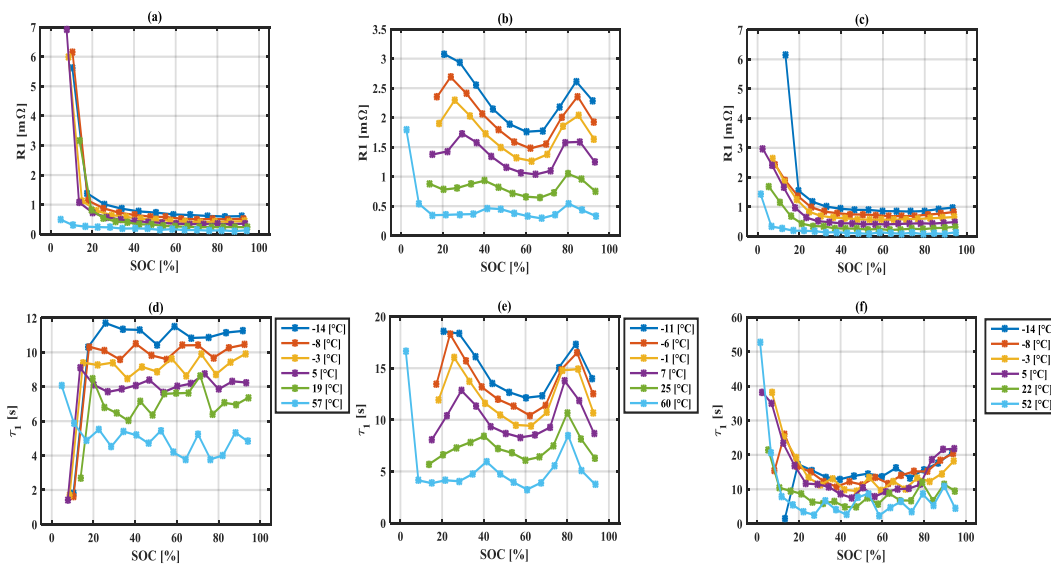


Figure 4.8: RC link parameters for 1RC model (a) 'N1' (b) 'M1' (c) 'T3'

4.3 Model Verification

Figures 4.9, 4.10 and 4.11 shows electrical model comparison for all three cells. It is apparent that the 1RC and 2RC model works better and follows the measurement value in most cases, while the 0RC model deviates a lot from the measurement data due to the significant effect of diffusion voltage discussed in section 2.4. The 0RC model does not capture the electrical dynamic behaviour in the cell system unlike the 1RC and 2RC model.

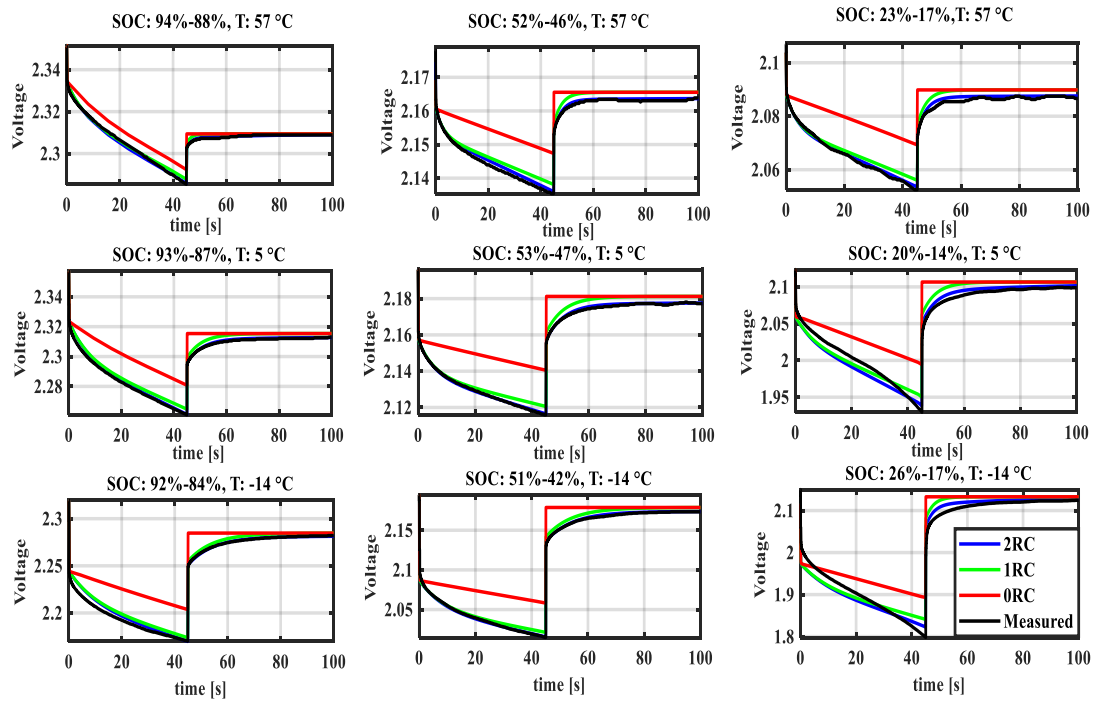


Figure 4.9: Model verification of 'N1' cell

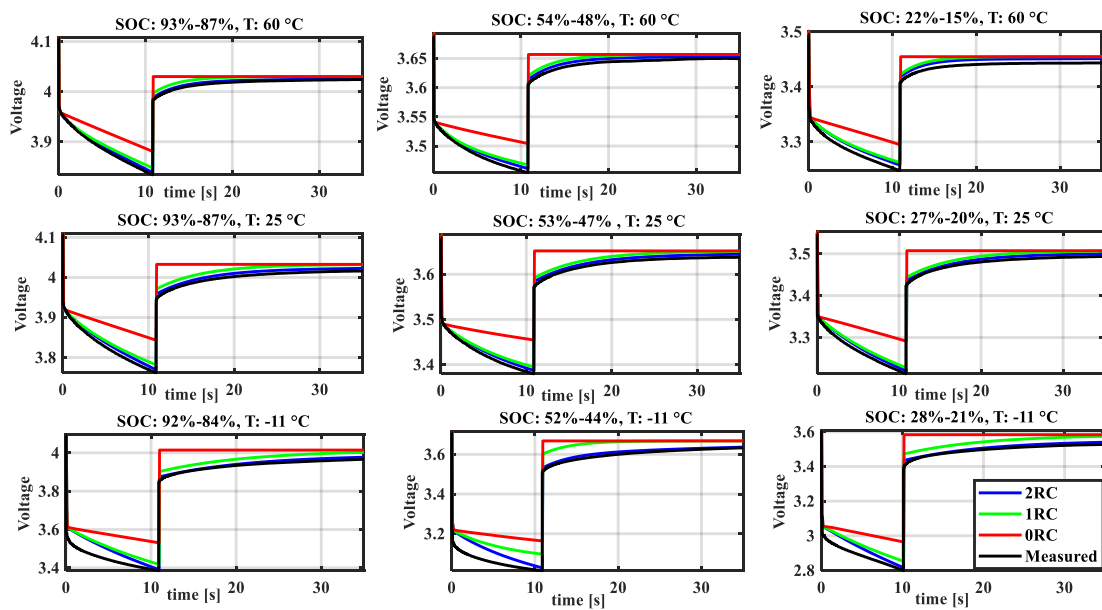


Figure 4.10: Model verification of 'M1' cell

4. Results

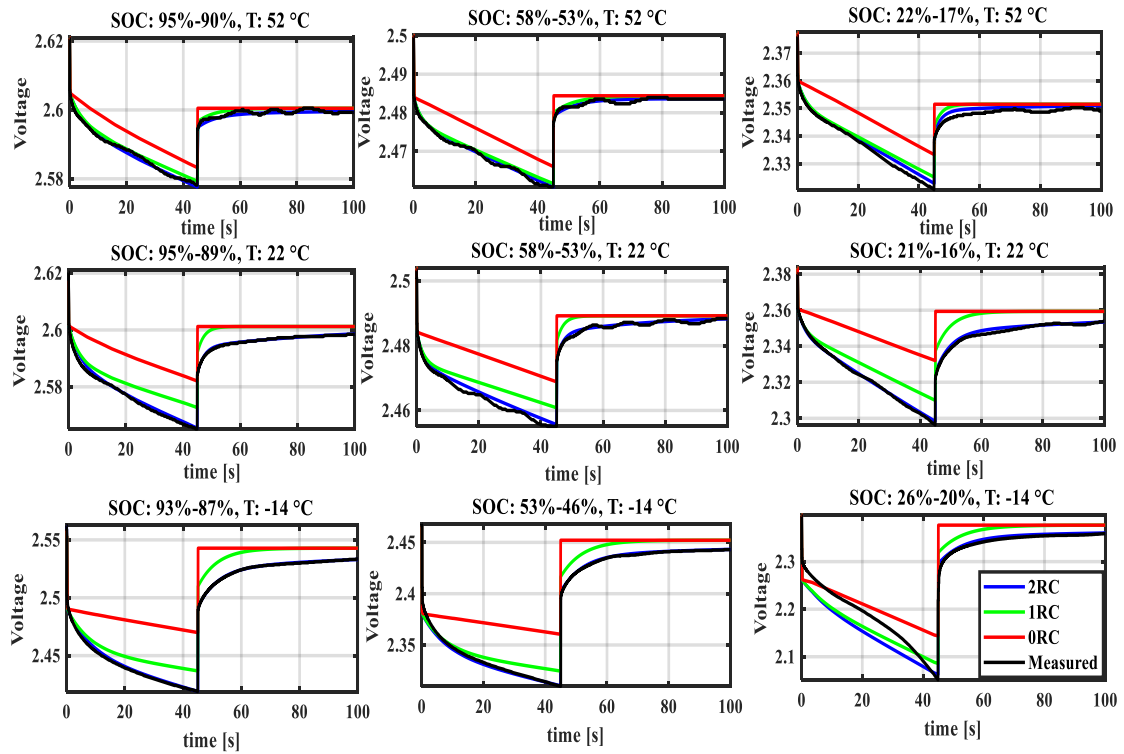


Figure 4.11: Model verification of 'T3' cell

The accuracy of the model in percentage is studied by plotting the voltage RMSE on the left y axis and $RMSE/V_{nom}$ on the right y axis. The RMS error comparison for the N1, M1, T3 cells are shown in figures 4.13, 4.14, 4.14 respectively. In these figures the 0RC, 1RC, 2RC graphs are shown in red, pale blue and pale green colour respectively. It can be noted that the 2RC model has slightly lower RMSE when compared to 1RC model. Also it is evident that the 0RC model has highest error across almost all SOC and temperature levels.

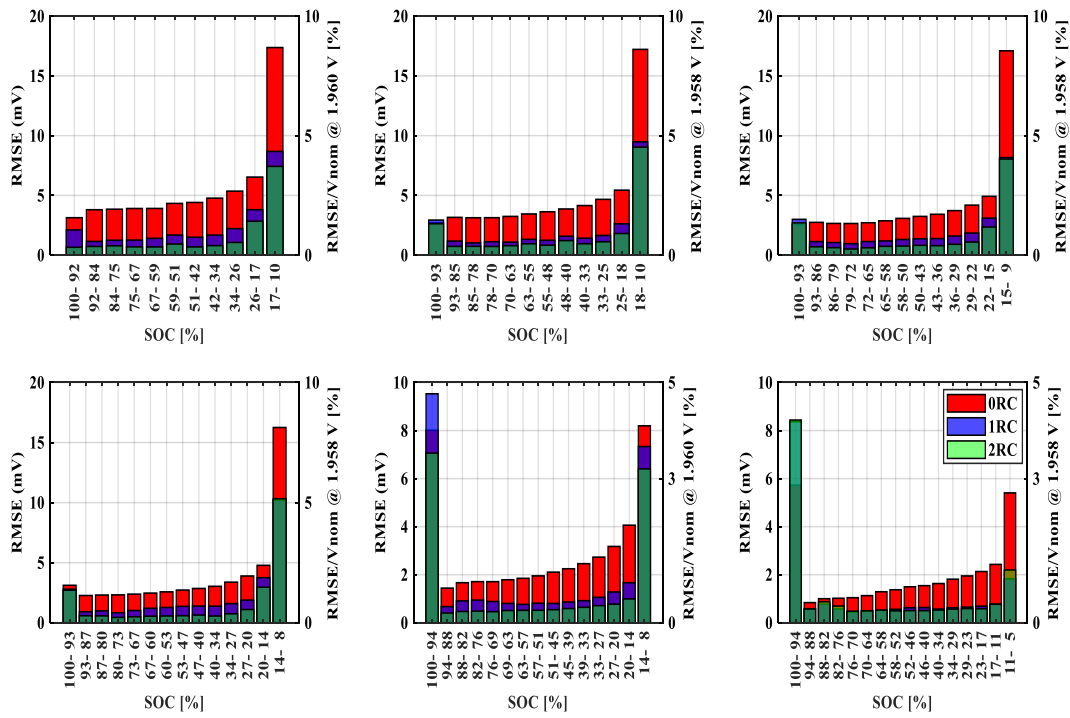


Figure 4.12: RMSE comparison for N1 cell

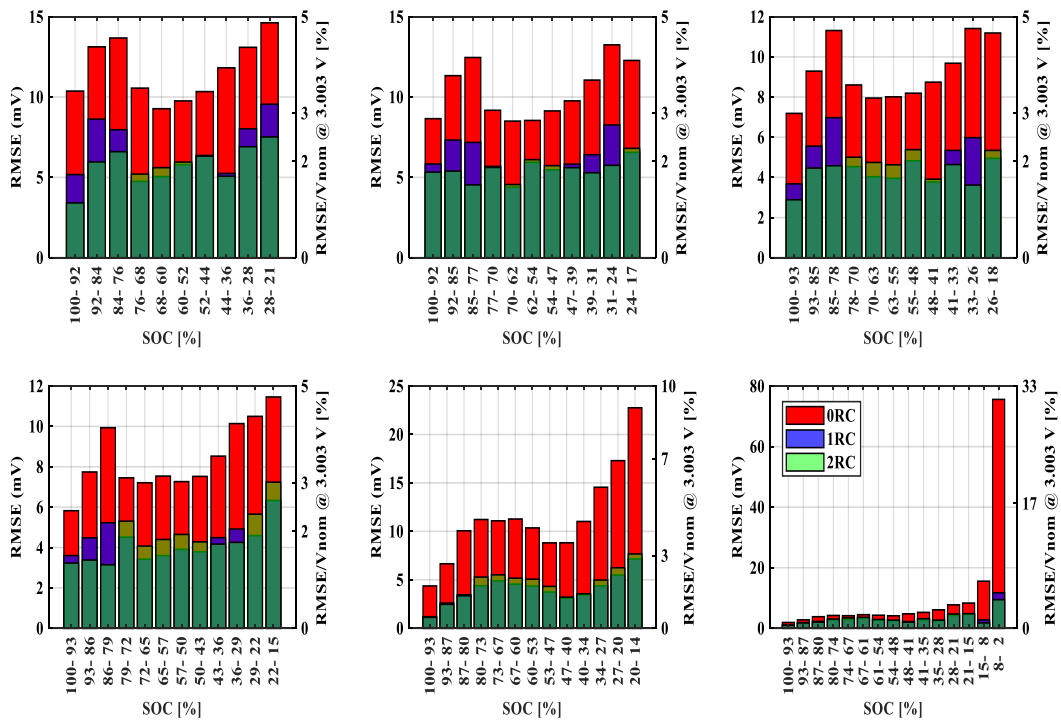


Figure 4.13: RMSE comparison for M1 cell

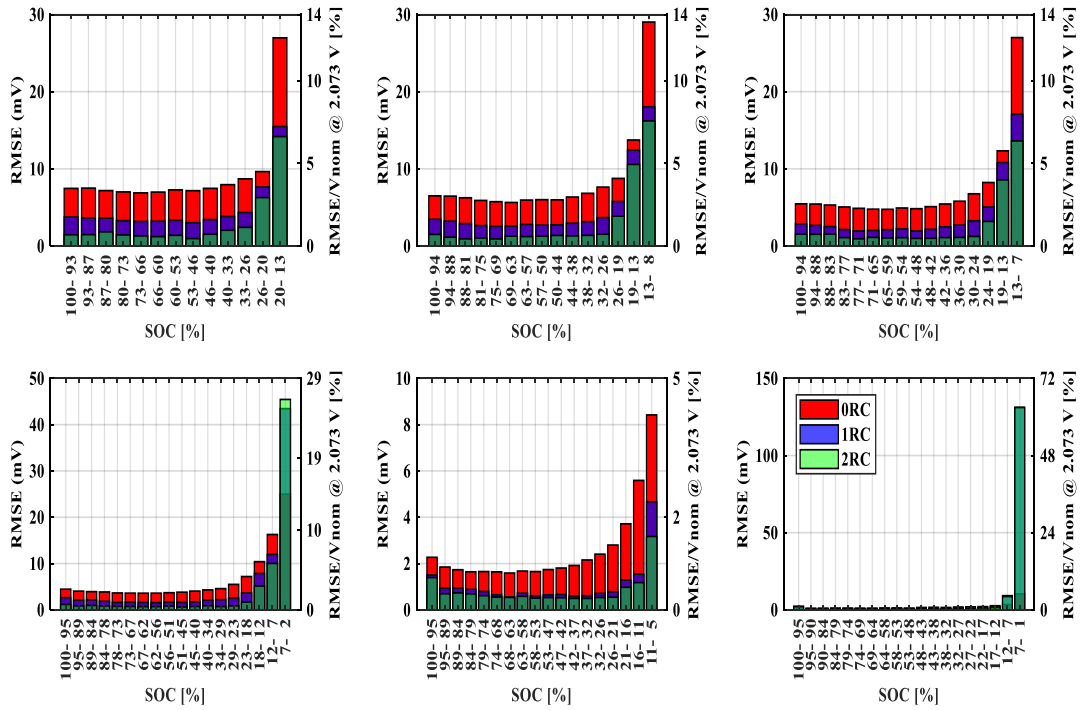


Figure 4.14: RMSE comparison for T3 cell

4.4 Battery Pack Simulations

Figure 4.15 shows the voltage, current, SOC and temperature of battery pack model for a double WLTP cycle. The battery pack model has 24 cells with a 12s2p cell configuration of 'M1' NMC cells. The battery voltage is normalized with respect to the nominal battery voltage, current is normalized with respect to RMS current and the SOC is normalized with respect to SOC range. The SOC range is typically around 50%.

The RMSE voltage for the 1RC and the 2RC model is roughly 500 mV, which corresponds to 1% of the nominal voltage. Therefore the 1RC electrical model should be good enough to represent the battery pack electrical behavior. The maximum error of the electrical model is 6% which occurred at low temperature. This is expected since the starting temperature of the double WLTP cycle is lower than the lowest temperature that the cells was tested for. Battery resistance will increase significantly for lower temperatures, hence in order to improve the model some extrapolation of the R_0 resistance is done by plotting the total battery pack resistance for several driving cycles at low temperatures. Before the extrapolation of the R_0 resistance the maximum error was 8.6%.

In case of SOC, the simulated value matches the measured value approximately. One explanation for the SOC deviation could be the fact that the current measurements

were recorded with 2Hz frequency, and therefore some transient high current peaks might have been missed out in between the measurements. Another factor could be the charging efficiency of the battery which is neglected in this model. The RMSE of the SOC is 1% for the double WLTP driving cycle, and the maximum error is 2%. The 1D-lumped parameter thermal model is able to predict the temperature fairly well. The RMSE of the temperature for the double WLTP is 1°C, while the maximum error was 4°C. It is expected that the thermal model will have some errors since the 1D-lumped parameters model assumes that the temperature of the battery pack is spatially uniform, which is not the case.

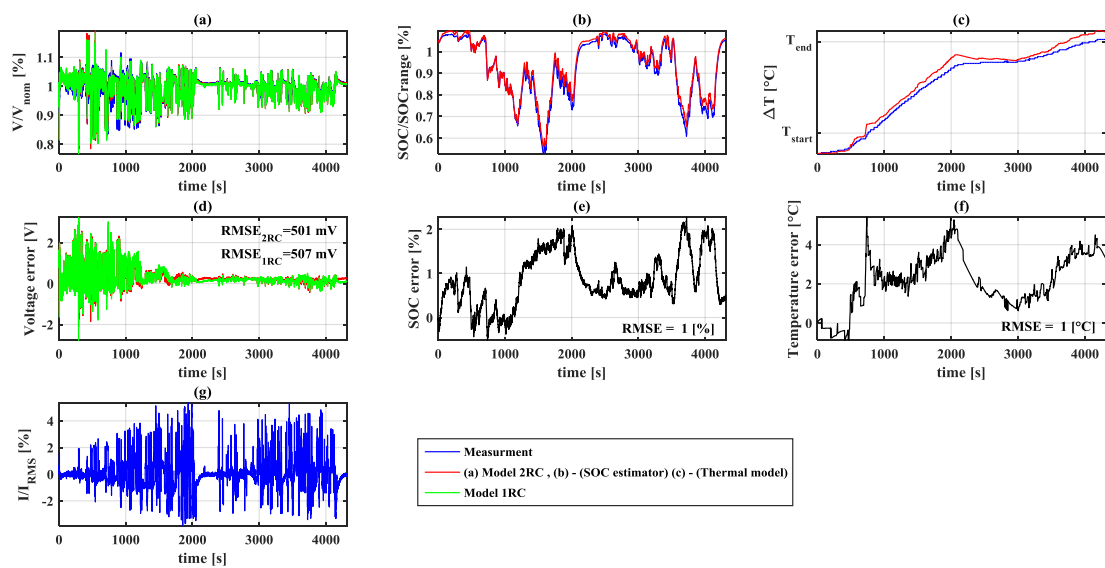


Figure 4.15: Battery pack model for a WLTP driving cycle (a) Battery Voltage / Nominal Voltage, (b) SOC/SOCrange, (c), (d) Temperature, (e) Voltage error, (f) SOC error, (g) Temperature error

Figure 4.16 shows RMSE values for voltage, SOC and temperature for different driving cycles. For the electrical model, the aim to reduce the $RMSE/V_{nom}$ below 1.5% is reached for all the driving cycles. It is clear that in terms of electrical model the 1RC and the 2RC model performance are similar, and both are slightly better than the reference model. The SOC estimator produces RMSE of 1%-2% for an entire drive cycle, which would be acceptable. The SOC estimator also performed slightly better than the reference model. For the thermal model it can be concluded that the 1D-lumped parameter model produced an RMSE value between 1°C and 2°C.

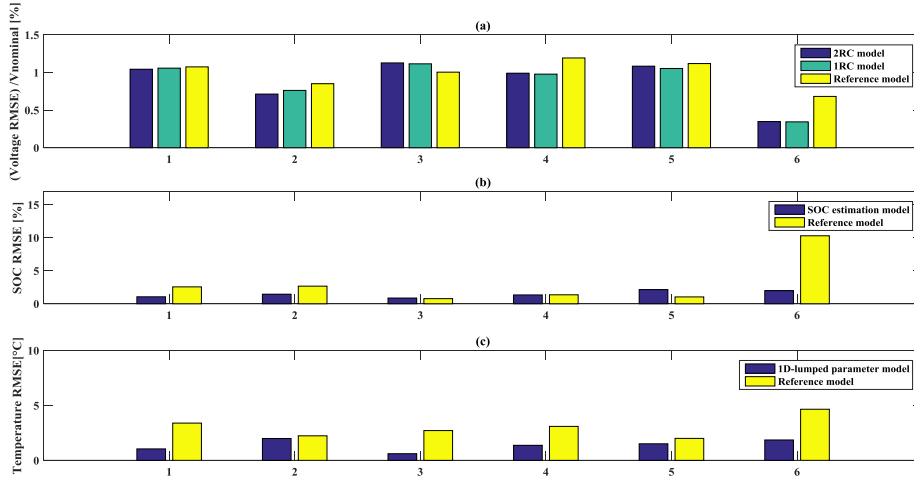


Figure 4.16: (a) RMSE value for Voltage, (b) SOC, (c) Temperature for the different driving cycles

4.5 System Simulations

Figure 4.17 shows the system simulation plots for battery current, voltage, SOC and temperature for a WLTP driving cycle. It is observed that the measured and the simulated current for both the IGSM and the battery pack follows each other approximately. The voltage RMSE is 341 mV for this driving cycle and the maximum error is 2.9 V. Thus it can be concluded that the electrical battery pack model still render accurate voltage estimation when implemented in a more complex simulation environment. The maximum SOC error is 3% with a SOC RMSE of 1%, the possible reasons for the deviation in SOC are discussed in section 4.4.

The temperature RMSE is much higher since only the initial ambient temperature is known for this WLTP cycle. In the performed simulations as in section 4.4, the ambient temperature was known and could be feed to the model. Therefore a transfer function is used to model the ambient temperature increase instead of feeding measurement data to the model. Therefore higher temperature error is expected.

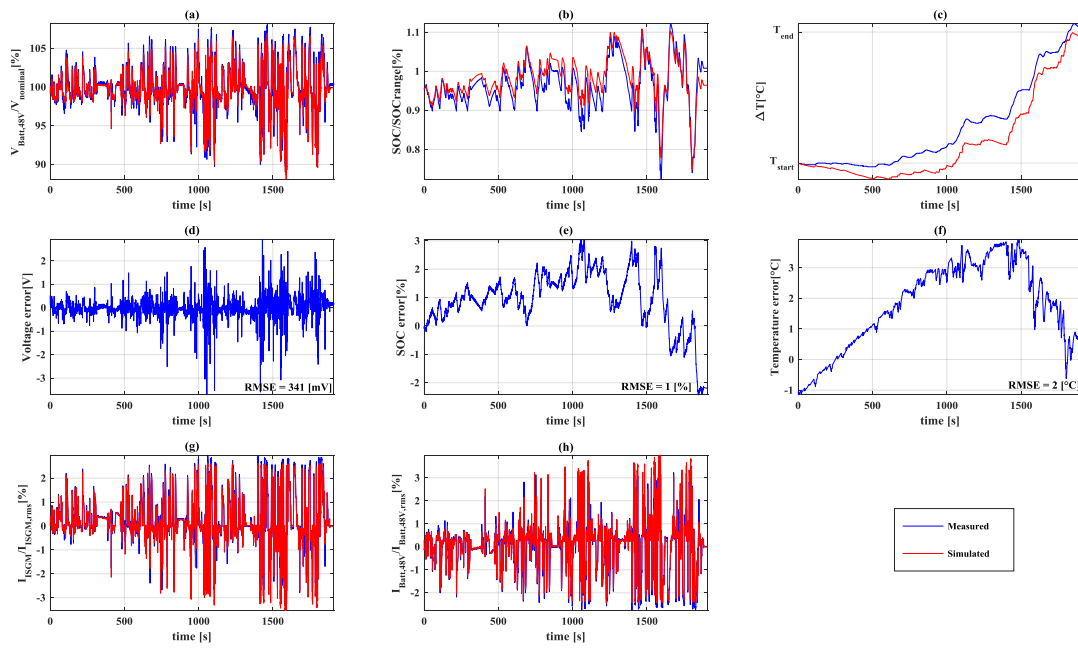


Figure 4.17: 48 V board net simulation (a)Battery Voltage (b)SOC (c)Temperature (d)Voltage Error (e)SOC Error (f)Temperature Error (g)ISGM current (h)Battery Current

5

Conclusion

Based on the presented results and the discussion above, some conclusions are drawn from the study. These conclusions are presented in the sections below, followed by some interesting topics for future research.

5.1 Cell chemistry comparison

From the cell measurement data it can be concluded that the LTO cells are retaining more of their capacity compared to the NMC cell for lower temperatures. By analyzing the equivalent resistances of the cells, it is concluded that the LTO cells have less mass transport and thus react electrochemically faster than the NMC cell. When comparing cell resistance versus SOC it is concluded that the NMC cells' resistance vary less with SOC than the LTO cells.

5.2 Electro-thermal battery pack model evaluation

The developed electro-thermal battery pack model is able to predict both voltage, SOC and temperature well during drive cycle behavior. The RMSE/Nominal voltage is less than 1.5% while the SOC and the temperature RMSE is less than 2% during different tested drive cycles. The comparison between 0RC, 1RC and 2RC electrical model is conducted on a cell level. It is found that there is only a minor difference between an 1RC and 2RC model, while the 0RC model produces a significantly higher error during pulse verification.

5.3 Sustainable aspects

Several studies have shown a promising outlook for the 48 V based mild hybrid. Depending on the engine placement, the mild hybrid has the potential to increase fuel efficiency from 7%-16% for a WLTP cycle according to [8]. In [29], an ideal P2 mild hybrid could reduce the fuel consumption by 40.7% for city driving compared to a micro hybrid. Features such as torque assistance, regenerative braking and the start-stop system of the mild hybrid can help car manufacturers reach the goal of 95 grams of CO_2 per kilometer by 2021. Also, the 48 V system requires lower current than the 12 V system and therefore needs smaller diameter cable to carry current,

which in turn reduces the weight and copper losses. The 48 V Li-ion battery pack is one of the key components of the mild hybrid in terms of performance and fuel savings. Looking at figure 4.2, 4.3 and 4.4 it is clear that the LTO cells have lower internal resistance, and react electrochemically faster than the NMC cell. Evaluating the cell capacity vs temperature in figure 4.1, the LTO cell 'T3' has the highest capacity retention. These are important factors when considering the most sustainable choice of cell chemistry since it is directly related to the battery performance. However, when evaluating the battery pack, all steps in the life cycle need to be considered, starting from mining the materials, to manufacturing processes, lifetime usage, and waste management.

5.4 Ethics

In this research, the IEEE code of ethics has been applied. According to the IEEE code of ethics one must be honest and realistic in stating claims or estimates based on available data [30]. It is important to be as objective as possible when presenting the results of the research in order to not mislead the reader. Also, the IEEE code of ethics states that one should seek, accept, and offer honest criticism of technical work, to acknowledge and correct errors, and to credit properly the contributions of others. This has been achieved by having a continuous dialogue with supervisors, embracing their feedback and acknowledge their support. Finally, the IEEE code of ethics states that one must avoid injuring others, their property, reputation, or employment by false or malicious action. This has been achieved by being loyal to VCC and Chalmers University of Technology and their regulations, honoring the disclosure agreements and publishing only non-confidential data.

5.5 Future work

In this study, the parameter dependencies taken in to consideration are SOC and temperature. In reality, battery performance also depends on several other factors such as current and age. It could be interesting to see how the electrical parameters varies with current and age as well.

Further, capacity degradation is not considered in this study. It could be of interest to expand the model and include state-of-health (SOH) as an input to the model for simulating the battery pack behaviour.

In this thesis only a brief comparison between the electrical behavior of the LTO cells and the NMC cell are conducted. Since the cells have different chemistries, a more detailed study about the cell chemistry would be preferable in order to evaluate which cell that is most suited for the 48 V battery in a mild hybrid. When comparing cells, factors such as energy density, power density, safety, price and cycle life could be taken in to consideration.

Bibliography

- [1] Europa Commission, Reducing CO2 emissions from passenger cars , 2018. [Online]. Available: https://ec.europa.eu/clima/policies/transport/vehicles/cars_en, Accessed on: 2018-01-24
- [2] "An Approach for Vehicle Electrification - IEEE Transportation Electrification Community", Tec.ieee.org, 2018. [Online]. Available: <https://tec.ieee.org/newsletter/january-february-2015/an-approach-for-vehicle-electrification>. [Accessed: 16- Mar- 2018].
- [3] O. Copping, Eehe.de, 2018. [Online]. Available: http://eehe.de/wp-content/uploads/2017/05/COPPIN_VALEO_Modular_EE_Architectures_for_hybridization_EEHE_2017_VF.pdf. Accessed: 29- Jan- 2018
- [4] R. Bao, V. Avila, J.Baxter, "Effect of 48 V Mild Hybrid System Layout on Powertrain System Efficiency and Its Potential of Fuel Economy Improvement" [Online]. Available: <https://saemobilus.sae.org/content/2017-01-1175> Accessed on: 2018-01-26
- [5] "Volvo Cars to go all electric", Media.volvocars.com, 2017. [Online]. Available: <https://www.media.volvocars.com/global/en-gb/media/pressreleases/210058/volvo-cars-to-go-all-electric>. [Accessed: 07-May- 2018].
- [6] "Mild Hybrid Electro-Thermal Battery Modelling", Master of Science Thesis, Chalmers University of Technology, 2016.
- [7] S. Chacko and Y. Chung, "Thermal modelling of Li-ion polymer battery for electric vehicle drive cycles", 2018. .
- [8] "Mild Hybrid Electric Vehicle (MHEV) – architectures – x-engineer.org", X-engineer.org, 2018. [Online]. Available: <https://x-engineer.org/automotive-engineering/vehicle/hybrid/mild-hybrid-electric-vehicle-mhev-architectures/>. [Accessed: 16- May- 2018].
- [9] D. Dörsam, D. Kehl, D. Klinkig, D. Radon and D. Sirch, The new voltage level 48 V for vehicle power supply, 7th ed. Germany: Springer Vieweg | Springer Fachmedien Wiesbaden GmbH, 2018, p. 6.
- [10] A. Weber, "48-Volt Systems Will Help Reduce Wiring Costs", assemblymag, 2015. [Online]. Available: <https://www.assemblymag.com/articles/93092-volt-systems-will-help-reduce-wiring-costs>. [Accessed: 16- May- 2018].
- [11] Sebastian Larqvist, Hannes Östergren "Electric Machine Comparison for Mild Hybrid Light Vehicles with Respect to Performance and Thermal Capability"

- [12] R. Bao, V. Avila and J. Baxter, "Effect of 48 V Mild Hybrid System Layout on Powertrain System Efficiency and Its Potential of Fuel Economy Improvement", 2018.
- [13] H. Fischer and D. Korthauer, 48-Volt Electrical Systems- A key Technology paving to the road to Electrical Mobility. Germany: ZVEI-German Electrical and Electronic, 2016, p. 40.
- [14] L. Brusokas and N. Rajarathinam, "Evaluation of Electrical Loads on 48 V Supply in Future Mild Hybrid Electric Vehicles", Chalmers studentarbeten, 2018. [Online]. Available: <http://studentarbeten.chalmers.se/publication/221240-evaluation-of-electrical-loads-on-48-v-supply-in-future-mild-hybrid-electric-vehicles>.
- [15] "Williamson - Energy Management Strategies for Electric and Plug-in Hybrid Electric Vehicles (2013).pdf | Electric Vehicle | Plug In Hybrid", Scribd, 2018. [Online]. Available: <https://www.scribd.com/document/359199150/williamson-energy-management-strategies-for-electric-and-plug-in-hybrid-electric-vehicles-2013-pdf>. [Accessed: 16- May- 2018].
- [16] H. Berg, Batteries for electric vehicles, 1st ed. Cambridge: Cambridge University Press, 2015.
- [17] G. Plett, Battery management systems. Volume 1, battery modeling. Boston: Artech House, 2015.
- [18] S. Skoog, "Parameterization of equivalent circuit models for high power lithium-ion batteries in HEV applications", in 18th European Conference on Power Electronics and Applications (EPE'16 ECCE Europe), Karlsruhe, Germany, 2016.
- [19] A. Thaler and D. Watzenig, Automotive battery technology. Springer, 2014.
- [20] "Charging Lithium-Ion Batteries", Batteryuniversity.com, 2018. [Online]. Available: http://batteryuniversity.com/learn/article/charging_lithium_ion_batteries. [Accessed: 12- May- 2018].
- [21] S. Skoog, "Electro-thermal modeling of high-performance lithium-ion energy storage systems including reversible entropy heat", Applied Power Electronics Conference and Exposition (APEC), 2017 IEEE, 2017.
- [22] "What is WLTP: the Worldwide Harmonised Light Vehicle Test Procedure? | WLTPfacts.eu", WLTPfacts.eu, 2018. [Online]. Available: <http://wltpfacts.eu/what-is-wltp-how-will-it-work/>. [Accessed: 09- May- 2018].
- [23] Team, MIT Electrical Vehicle "A Guide to Understanding Battery Specifications" (2008)
- [24] Lijun Zhang, Hui peng, Zhansheng Ning, Zhongqiang Mu and Chanyan Sun, "Comparative Research on RC Equivalent Circuit Models for Lithium-Ion Batteries of Electric Vehicles" 2017.
- [25] F. P. Incropera and D. P. DeWitt, Introduction to Heat Transfer, 6th ed. 2011.
- [26] Another look at measures of forecast accuracy | Rob J Hyndman", Robjhyndman.com, 2018. [Online]. Available: <https://robjhyndman.com/publications/another-look-at-measures-of-forecast-accuracy/>.

- [27] A. Hausmann and C. Depcik, "Expanding the Peukert equation for battery capacity modeling through inclusion of a temperature dependency", *Journal of Power Sources*, vol. 235, pp. 148-158, 2013.
- [28] Y. Ji, Y. Zhang and C. Wang, "Li-Ion Cell Operation at Low Temperatures", *Journal of the Electrochemical Society*, vol. 160, no. 4, pp. A636-A649, 2013.
- [29] S. Skoog, "Experimental and model based evaluation of mild hybrid fuel consumption gains and electric machine utilization for personal vehicle application", 2017.
- [30] "IEEE Code of Ethics", *Ieee.org*, 2018. [Online]. Available: <https://www.ieee.org/about/corporate/governance/p7-8.html>. [Accessed: 17- Jun- 2018].